Louisiana State University

LSU Digital Commons

2011

Photoelectrochemical etching of isolated, high aspect ratio micorstructures in n-type silicon (100)

Purnima Narayanan
Louisiana State University and Agricultural and Mechanical College

Follow this and additional works at: https://digitalcommons.lsu.edu/gradschool_theses

Part of the Chemical Engineering Commons

PHOTOELECTROCHEMICAL ETCHING OF ISOLATED, HIGH ASPECT RATIO MICROSTRUCTURES IN n-TYPE SILICON (100)

A Thesis

Submitted to the Graduate Faculty of the
Louisiana State University and
Agriculture and Mechanical College
in partial fulfillment of the
requirements for the degree of
Master of Science in Chemical Engineering

in

The Gordon A. and Mary Cain Department of Chemical Engineering

by

Purnima Narayanan
B.E., University of Mumbai, 2007
August 2011

ACKNOWLEDGEMENTS

TABLE OF CONTENTS

LIST OF FIGURES

ABSTRACT

Three-dimensional integration techniques have become increasingly popular to meet the ever rising demand of high capacity and reduced package size in microelectronics devices. Through Silicon Vias (TSVs) offer an efficient method to achieve 3D packaging with shorter interconnection length and higher interconnect density relative to conventional wire bonding. Wet electrochemical etching is a simple technique which may be used to create deep structures in silicon and is relatively low cost compared with Reactive Ion Etching or Laser drilling. Historically, a primary challenge is passivating TSV (macropore, microstructure) sidewalls against etching at sidewall thickness greater than twice the depletion region width. Lehmann et al created macropores in n-type silicon (40 Ω-cm) with sidewall thickness ~ six times depletion region width, however the wall surface smoothness differed from the macropores passivated by the depletion region. In this research, an attempt was made to create isolated (sidewall thickness = ∞ times the depletion region width) microstructures in patterned n-type silicon (100). For the first time, high aspect ratio (~5:1) deep microstructures with non-porous sidewalls at isolated pitches (>100 µm) are demonstrated using frontside illumination with photoelectrochemical etching. Further, the microstructure aspect ratio is observed to increase with etch duration. While literature on backside illumination illustrates porous sidewalls at isolated pitches, results from this study show frontside illumination can be used to create non-porous microstructures at large pitches. The microstructure etch rate is a function of light intensity and supporting electrolyte composition whereas the microstructure sidewall etching is demonstrated to be a function of applied anodic bias. Anodic bias controls the depletion region width which governs the dominance of drift and diffusion currents. Isolated microstructures are obtained at a low anodic bias where silicon dissolution is controlled by the diffusion current. The microstructure surface

smoothness is affected by incident light wavelength; sidewall roughness is minimized by conducting the dissolution reaction with photons having shallower absorption depth in silicon. The work shows photoelectrochemical etching of isolated, anisotropic, high aspect ratio microstructures is possible using frontside illumination with low wavelength light at low anodic bias.

1   INTRODUCTION

For more than four decades the semiconductor process development has followed Moore's law, however this law faces limitations as technology approaches atomic dimensions. Moore's law predicts the number of transistors in a microprocessor will approximately double every two years (Moore 1965). Increase in the number of transistors in a small area leads to problems involving power consumption, and transmission speed in 2D inteconnected systems. 'More than Moore' law suggests 3D integration schemes can resolve the large scale integration issue with 2D packaging using vertical interconnection schemes (Saadaoui, Wien et al. 2008). 3D interconnections increase the functionality of the microprocessors by decreasing distance between the transistors. 3D Interconnection is realized by System in Package (SiP) and Through Silicon Vias (TSVs) (Figure 1.1). SiP connects the die using wire bond or solder bump technology. Unlike SiP, TSVs create interconnections through the body of the die thereby decreasing the overall device size. TSV combines advantages of both System on Chip (SoC – 2D packaging) and SiP to deliver devices with high speed and reliability, and smaller size and low power consumption (SEMATECH).
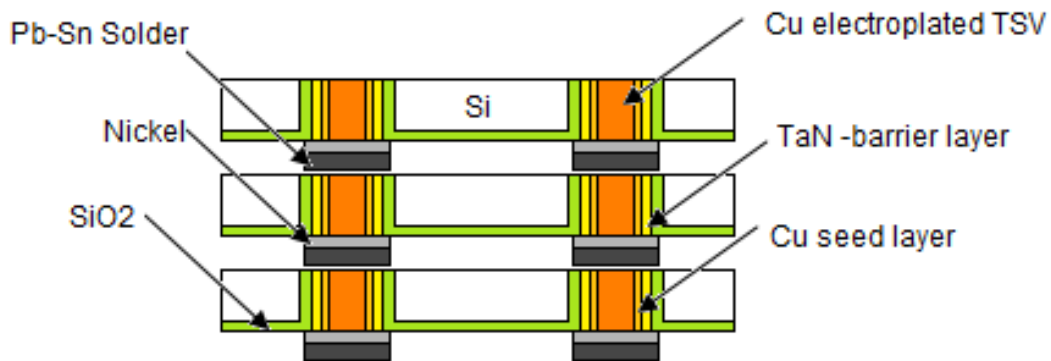
Figure 1.1. 3D Packaging Schematic.

Figure 1.2. Copper filled TSVs. Reference Van Olmen et al., "3D Stacked IC Demonstration using a Through Silicon Via First Approach", IEEE Conference Proceedings publication (© 2008 IEEE).

TSVs are high aspect ratio anisotropic structures developed in silicon (Si). These structures are backfilled with highly conductive metal for vertical interconnection (Figure 1.2). 'Deep Reactive-Ion Etching' (DRIE) process is widely adopted by semiconductor industries to form TSVs. Though DRIE is currently best foreseeable choice for TSV fabrication in 3D interconnects, this technique is still drawn back with some undesirable attributes such as scalloped sidewalls, greenhouse gas emission, increased production cost, low throughput, and low etch rates in deep structures. On the other hand, wet electrochemical etching is a simple, and low cost process to create TSVs. The electrochemical etching process has lower energy requirement compared to DRIE. Use of HF and its waste disposal is more controllable and environment-friendly than SF_6. Hence, wet electrochemical etching can prove to be viable solution for the problems related to cost and environmental pollution posed by DRIE.

In 3D interconnection, devices are electrically connected by filling TSVs with conductive material. Si processing temperature is high and while cooling, rate of contraction of copper filled TSVs is faster than the surrounding Si. The difference in the silicon and copper cooling

2

rate leads to mechanical stress in bulk Si around the TSVs. Stress hinders the device performance and can even result in mechanical failure (Lu, Xuefeng et al. 2009). The stress developed in Si can be alleviated by locating the TSVs at larger pitches (100-500 µm). A sidewall thickness of 38-40 µm between adjacent TSVs is demonstrated via wet electrochemical etching process (Lehmann and Ronnebeck 1999).

Wet photoelectrochemical dissolution of n-type Si can be achieved by both frontside and backside illumination. During frontside illumination, charge carriers are generated near silicon-electrolyte surface whereas backside illumination gives rise to charge carriers in bulk silicon. It is found that trench growth is promoted only when the charge carriers are present in the bulk and near-surface charge carriers lead to lateral expansion of the trenches (Lehmann and Foll 1990). This led to backside illumination being preferred over frontside illumination for creation of deep trenches. While this argument is valid for tight pitches, we run into the problem of side wall etching as we move to isolated pitches. When the pattern to be etched has wall thickness greater than twice depletion region width, presence of holes in the bulk silicon will lead to side-wall branching. Near-surface holes generated with frontside illumination can alleviate the problem of sidewall branching. In this work, we deduce the conditions to fabricate anisotropic, high aspect ratio, isolated TSVs via wet photoelectrochemical etching using frontside illumination. Anodic bias applied for the electrochemical dissolution and wavelength of the illumination source form key parameters for fabricating isolated, high aspect ratio TSVs.

In the further sections of this thesis we will refer to TSVs as microstructures (vias, trenches, spirals, etc.) due to their wide range of application not only in microelectronics but also in micro-electro-mechanical systems, microfluidics, and photovoltaics.

3

2   BACKGROUND AND LITERATURE SURVEY

2.1 Background and Band Structure of Silicon Electrolyte Interface

Silicon (Si) may be classified into n-type or p-type based on the dopant introduced. Addition of group V elements, namely, Phosphorus, Antimony or Arsenic in Si provides excess electrons hence, named n-type; while doping silicon with group III element such as Boron, causes it to be p-type. The electronic structure of Si is understood in terms of energy bands composed of atomic orbitals of the individual atoms. Free electrons lie in the conduction band and holes form medium for electrical conduction in the valence band. Band gap is the energy difference between the conduction band and valence band. Band gap of silicon at room temperature is 1.12 eV. If Si is externally supplied with energy equivalent to the band gap energy electron hole pairs can be generated. As the external energy exceeds the band gap energy, an electron bound to the Si lattice acquires enough energy to break the covalent bond and be a part of the conduction band. This creates a vacancy – hole in the valence band of Si. Thus, the band structure of Si is comprised of higher electron energy conduction band and lower electron energy valence band. The change in the Gibbs energy of a charged particle in a system of charged particles is defined as the electrochemical potential of that system (Sato 1998). The electrochemical potential of a semiconductor (charged particles = electrons) is known as the Fermi energy. At absolute zero, Fermi level is designated as the energy level where no electrons in the material will have the energy to rise above this level. Electrons with greater energy than Fermi energy may be available for conduction; electrons with less energy are bound to the crystal structure. Position of the Fermi level varies with the type and amount of active dopant introduced. For an electrolyte, the redox potential is the electrochemical potential. When a semiconductor-electrolyte interface is at equilibrium, the electrochemical potentials of the two phases are equal. The redox potential of

most electrolytes lies in between the band gap of the semiconductor that is in between bottom of the conduction band and top of the valence band. For a moderately doped (dopant concentration $< 10^{17} cm^{-3}$) n-type semiconductor, the fermi energy level is very close to the conduction band. For equilibrium to be established between two phases, electrons from n-type semiconductor are transferred into the electrolyte. Positive donor ions are left behind to some finite distance within semiconductor starting from the interface. This is reflected by the upward band bending at the interface. Charge transfer depends on the relative position of the Fermi level and the redox potential. Figure 2.1 illustrates the relative position of the Fermi level with respect to the electrolyte redox potential on application of an external bias. With n-type Si electrode, when a forward bias is applied, the Fermi energy is raised further higher as compared to zero bias equilibrium condition and electrons are transferred into the solution. An electron accumulation layer is formed if the surface reaction is slow or negligible, thus, bands bend downwards.
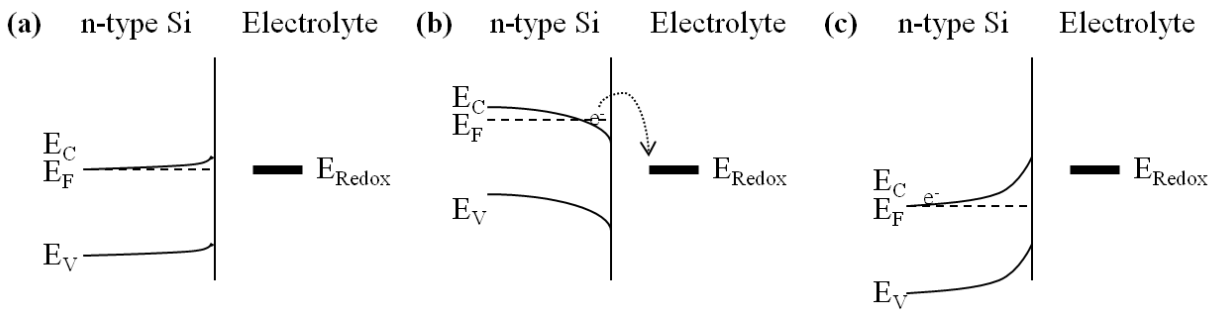
Figure 2.1. Energy band diagram at n-type silicon-electrolyte interface at (a) zero bias, (b) forward bias, and (c) reverse bias.

Alternately, application of a positive potential to n-type semiconductor with respect to equilibrium potential causes electron flow from the electrolyte into the semiconductor due to formation of space charge region (Więckowski 1999) also known as depletion region.

The energy band model gives the number of allowed states for an electron in each band. The number of states in the conduction and the valence band is given by the following equations:

$$g_C(E) = \frac{m_n^* \sqrt{2m_n^*(E-E_C)}}{\pi^2 . \hbar^3}, \text{ for } E \geq E_C \quad (2.1)$$

$$g_V(E) = \frac{m_p^* \sqrt{2m_p^*(E_V-E)}}{\pi^2 . \hbar^3}, \text{ for } E \leq E_V \quad (2.2)$$

Where, $g_C(E)$ and $g_V(E)$ are the density of states of conduction band and valence band, respectively, m_n^* and m_p^* are the electron effective mass and the hole effective mass, respectively, E_C and E_V are the minimum conduction band energy and maximum valence band energy, respectively and $\hbar = h/2\pi$ where, h is Plank's constant. The gap between the conduction band and the valence band is known as the forbidden energy gap. There are no energy states for the electron to occupy in the forbidden gap in an intrinsic semiconductor. Allowed energy states are created in the forbidden band when dopants are introduced in the semiconductor (Pierret 1996).

The allowed energy states in proximity to the material's surface are known as surface states (Interfacial traps or interface states). These energy states are localized (Pierret 1996). Si when exposed to air forms a native oxide layer on its surface. Presence of an oxide layer leads to excessive surface states in the form of dangling bonds giving rise to more electron-hole recombination centers. The surface oxide can be dissolved in HF and leaving the Si surface with H-terminated bonds. A lower density of surface states is reported with H-terminated silicon (Many, Wolovelsky et al. 1993; Savir, Many et al. 1995). The surface states charge and discharge based on the applied bias (Pierret 1996) and consequently influence the electrochemical dissolution process.

2.2 Alternative Techniques to Create Deep Microstructures in Silicon

The major techniques being studied to realize deep microstructures in Si are Alkaline etching, Deep Reactive Ion Etching (DRIE), Laser Drilling and Wet electrochemical etching.

➤ Alkaline etching:

Si can be anisotropically etched using KOH, NaOH, LiOH, ethylene diamine, and TMAH. KOH etching is commonly used to etch Si. The alkaline etchants etch the different crystals planes of Si with considerably different etch rates. The ratio of etch rate of Si(100) to Si(111) is 400 and that for Si(110) to Si(111) is 600 (Gad-el-Hak 2005). The etch rate variation with the crystallographic

Figure 2.2. SEM image showing the top view of a KOH pit in Si (100).

orientation causes anisotropy. When monocrystalline Si is subjected to alkaline etching at the (100) plane, inverted pyramid shaped structures are obtained as shown in Figure 2.2. Alkaline etching etches n-type and p-type silicon, also the etch profile remains constant for a given crystalline plane. Further, the alkaline etch profile is independent of the resistivity of the Si substrate. However, the major disadvantages of KOH etching is low aspect ratio and slanted sidewalls (sidewalls make an angle of 54.74° with the horizontal plane) (Barycka and Zubel 1995).

7

➢ DRIE - Bosch Process:

Conventional deep etching process for Si is a dry process using high density Inductively Coupled Plasma (ICP) etching systems. Bosch process consists of steps that alternate between reaction and passivation mechanisms. Commonly used dry etching gases are SF_6, NF_3 and CF_4. Passivation mechanism was initially developed as polymer deposition like CHF_3, C_4F_8 and Ar, (Franz Laermer 2002) and recently, hydrogen and oxygen (Sammak, Azimi et al. 2007; Sammak, Azimi et al. 2007) have been reported for the same purpose. Anisotropy of the structure is dependent on the etching and passivating gas flow rates and passivating time. A small deviation from optimal conditions leads to polymer deposition or isotropic etching (Blaw, Zijlstra et al. 2001). Advantages of the Bosch process are high aspect ratio TSV, stable repeatable etch profile, high etch selectivity and high etch rate (Wu, Kumar et al. 2010). Due to the alternating reaction-passivation mechanisms applied in DRIE scallops are formed on the sidewalls (Figure 2.3). These are not desired while metal filling. Also, the etchants mainly used are SF_6 and CF_4;
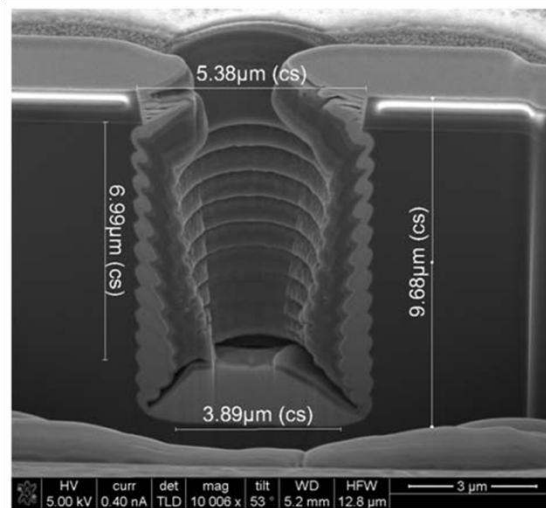
Figure 2.3. Through Silicon Via using DRIE technique, showing scalloped sidewalls. Reference Zhang et al., "Design, fabrication and electrical characterization of TSV", IEEE Conference Proceedings, Reprinted with permission from IEEE, (© 2010 IEEE).

SF_6 in particular is a highly potent greenhouse gas with 22,900 times more damaging effect than CO_2, while being stable in the atmosphere for 3,200 years, fluorocarbons are extremely toxic and bear a high cost. Many environmental and health issues like depletion of ozone layer and greenhouse effects are due to the existence of these compounds in the atmosphere. Besides these disadvantages, use of DRIE tool requires high energy that increases with production rate. Thus, the production cost escalates due to chemical costs as well as well as the energy requirements. Also, the etch rates attained depend on loading (exposed area) and aspect ratio. Large exposed area and deep features lead to slower vertical etch rate (Jansen, Gardeniers et al. 1996; M.Puech 2002). Major concern for industries using DRIE is incurred cost. The DRIE tool is complicated and the energy requirement scales with the production. Wet electrochemical etching systems on the contrary are comprised of simple reactor set up and inexpensive wet etching chemicals.

➢ Laser drilling:

Microstructures (Through Silicon Vias) can be formed in Si using Ultra Violet (UV) Laser drilling technique. Drilling is achieved with very high power density lasers. Etch depth attained depends on the number of shots. High etch rate per shot is achieved when microstructure diameter is small and the number of microstructures to be etched is less than 100 (Denda 2007).
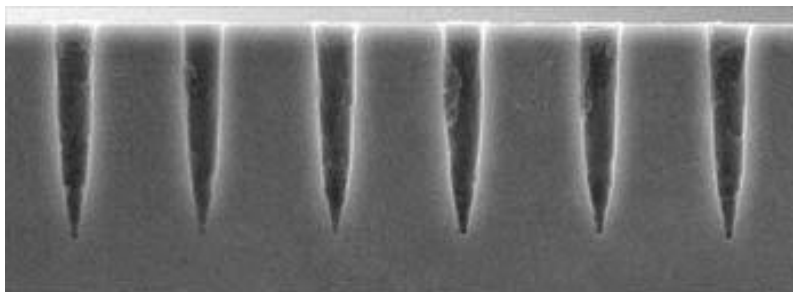
Figure 2.4. Microstructures in Si by Laser Drilling. Reference Rodin et al., "High Throughput Low CoO Industrial Laser Drilling Tool", Angel Business Communications. Reprinted with permission from EuroAsia Magazine.

4-20 µm/shot has been achieved using the laser ablation technique (Forsman, Lundgren et al. 2007; Rodin, Callaghan et al. 2008). The microstructure diameter is decided by aperture size on the Laser drilling equipment. This eliminates the requirement of expensive patterning steps that include Lithography and Reactive Ion etching (Sekiguchi, Numata et al. 2006). Tapered or U-shaped microstructures are obtained by laser ablation process (Figure 2.4) (Sekiguchi, Numata et al. 2006; Rodin, Callaghan et al. 2008). Laser drilling has some disadvantages that prohibit its wide scale industrial application. Whenever deep microstructures are created in Si during Back End of the Line (BEOL), silicon is placed on Aluminum wired substrate. Continuous laser action etches the underlying aluminum film (Denda 2007) leading to loss in device conductivity. The other concern is the excessive heat generated during the laser drilling process. Long exposure time leads to transmission of the heat generated to adjacent locations, and deters performance of the active devices. Also, it is difficult to remove condensed Si deposited on the microstructure walls after the drilling process.

Melt component, re-deposited material and thermal load on microstructures prevail even at extremely small laser pulse duration (50 ns). High energy laser and plasma exert tremendous pressure on silicon. This pressure increases mechanical load on Si decreasing overall process accuracy (Luft, Franz et al. 1996). Microstructure location and number depend on the laser drilling equipment positioning, making the process not suitable for high density input/output products.

➢ Wet photoelectrochemical etching:

Wet photoelectrochemical etching has the following advantages,

- All exposed regions are simultaneously etched.

- Experimental set up is simple and cost effective.

- Chemical (HF) waste management is easier as compared to green house gases emitted by DRIE process.

- Microstructure sidewalls are free of condensed silicon residue.

- No thermal effects are generated as extremely low light intensity light source is required for the process.

- Etch rate attained increases with diameter unlike Laser or DRIE process.

2.3 Classification of Electrochemically Etched Silicon

The structures created in Si by wet electrochemical etching using a fluoride source are classified based on their size. According to the IUPAC (International Union of Pure and Applied Chemistry) convention pores are classified into 3 categories based on their pore diameter; < 2 nm – micropores, 2 nm to 50 nm – mesopores, > 50 nm – macropores (Foll, Christophersen et al. 2002). In general, the term macropore is used for structures with diameter < 10 µm (Lehmann and Ronnebeck 1999; Al Rifai, Christophersen et al. 2000) but this terminology is not strictly followed. Larger pores or structures formed by merging of adjacent pores are called vias, trenches, or microstructures (Tao and Esashi 2005). Further, the surface of some of these structures are covered with filament like porous Si known as microporous Si (Zhang 2004) or nanoporous Si (Albuyaron, Bastide et al. 1993).

2.4 Mechanism of Silicon Etching

Si can be etched chemically and electrochemically using Hydrofluoric acid (HF). Since chemical etch rate of Si in HF solution is 0.3 Å/min (Hu and Kerr 1967; Peter, Riley et al. 1995), electrochemical dissolution is a must. Electron acceptors promote Si dissolution in acidic HF solution. In the absence of any other chemical oxidizer (electron acceptor), Si is forced to behave as an electron acceptor by applying a positive bias to the Si substrate. An electron can be injected
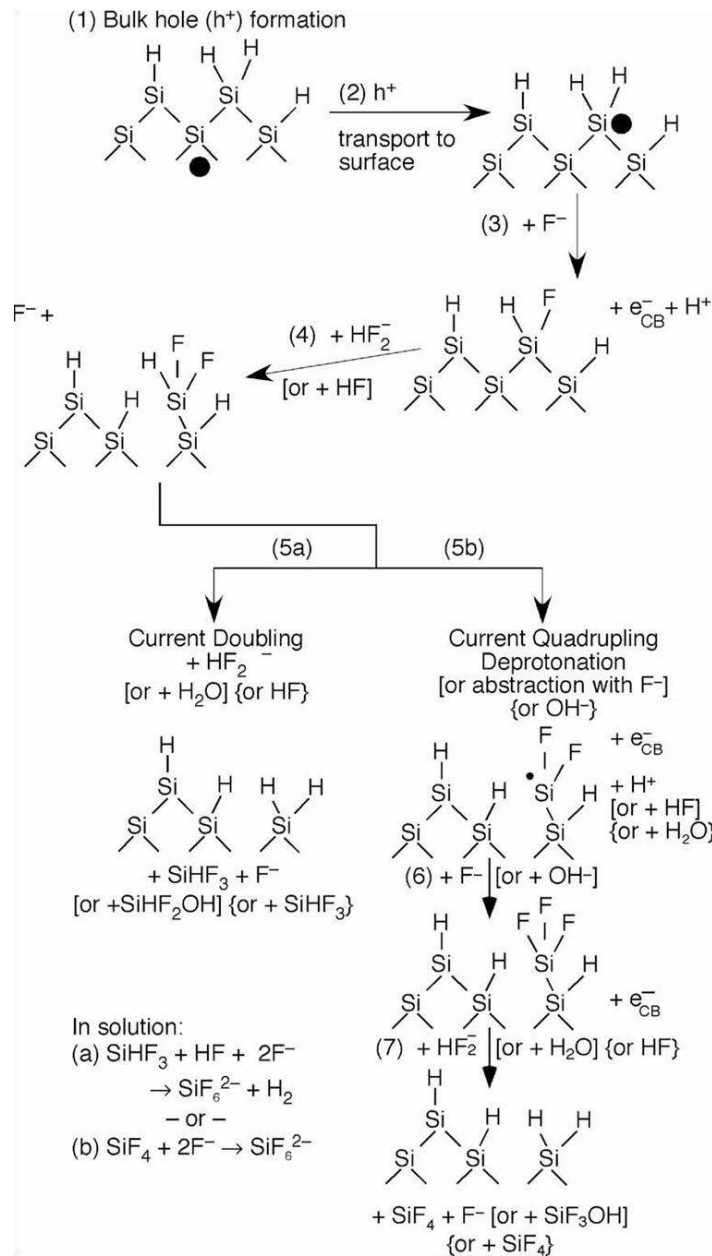
Figure 2.5. Modified Gerischer mechanism for Si etching in acidic fluoride solutions. Reprinted from Elsevier (Surface Science), Vol no 603, Kolasinski, Etching of silicon in fluoride solutions, No of pages 8, Copyright (2009), with permission from Elsevier.

in the conduction band of Si by providing energy greater than the band gap of Si or by hole recombination. Hole recombination process for electron transfer from the electrolyte occurs at energy lower than the band gap energy, hence, forms the first step of the etching reaction

(Lehmann and Gosele 1992). Holes in Si valence band represent a missing electron in the covalent bond between the Si atoms in the crystal. As the electron from the bonding orbital is removed the bond strength decreases. Thus, the presence of holes in valence band attracts a nucleophilic attack by weakening adjacent covalent bonds (Gerische.H and Mindt 1968). The application of an anodic bias leads to accumulation of holes at the silicon-electrolyte interface. Si immediately forms a native oxide layer when exposed to air. This native oxide can be dissolved in HF or any other fluoride source (Woodruff, Ratchford et al. 2007). Hydrogen-terminated silicon (Si-H) surface is obtained on dissolving this native oxide layer with a fluoride source. Si surface is not Fluorine-terminated because Si-F is a highly polar covalent bond. This high polarity of the Si-F bond weakens Si-Si backbonds and makes them prone to further chemical attack. Hence, Si-H bond which is close to a non-polar bond keeps Si in the crystal stable to further attack and thereby resulting in stable termination (Kolasinski 2009).

The Modified Gerischer mechanism for electrochemical etching of Si with an aqueous fluoride source is described by Kolasinski. Photon absorption during photoelectrochemical dissolution creates holes in the valence band of Si by transferring an electron into conduction band. Holes present in bulk Si are brought to silicon-electrolyte interface on application of an anodic bias. Substitution of H with F takes place since sticking coefficient of $F^-(aq)$ is increased by a large margin due to presence of holes at the interface. An electron is transported to the conduction band of silicon during this substitution. Thus, for every injected photon, two electrons are injected into the conduction band of Si leading to current doubling. Once Si-F bond is formed, polar nature of the bond weakens Si backbonds. HF or HF_2^- chemically attack the Si backbonds leading to dissolution. If the backbonds are attacked with F^- or OH^- present in electrolyte, two

additional electrons are injected into the conduction band of Si till a soluble SiF_6^{2-} species is formed. Thus, hydrogen abstraction or deprotonation by F^- or OH^- leads to current quadrupling. Over-all mechanism for silicon dissolution is as follows,

$$Si + 6HF + h^+ \rightarrow SiF_6^{2-} + 4H^+ + H_2 + e^- \quad \dots\dots\dots\dots\dots\dots\dots\dots\dots\dots\dots\dots\dots\dots(1)$$

$$Si + 6HF + h^+ \rightarrow SiF_6^{2-} + 6H^+ + 3e^- \quad \dots\dots\dots\dots\dots\dots\dots\dots\dots\dots\dots\dots\dots\dots\dots..(2)$$
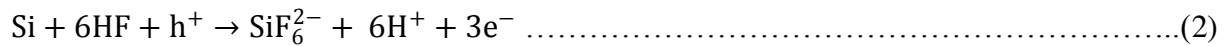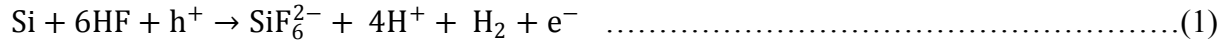
In both reactions (1) and (2), h^+ represents a hole in the valence band by photon absorption and an electron being injected into conduction band. Reaction (1) represents the over-all reaction for a current doubling process, whereas reaction (2) denotes a current quadrupling system. (Kolasinski 2009).

Studies on the mechanism of Si dissolution by aq. HF solutions suggest hole formation rate in Si and hole transport to the silicon-electrolyte interface remain as rate limiting steps for the overall Si dissolution reaction (Koker and Kolasinski 2001; Kolasinski 2003; Kolasinski 2009).

2.5 Hole Generation in n-Type Si

From the modified Gerischer mechanism of Si etching by Kolasinski, it is clear that (positive charge carriers) holes in Si valence band are essential for wet electrochemical dissolution in the presence of a fluoride source. Electrons being majority charge carriers in n-type Si, wet electrochemical etching cannot be carried out without additional steps to generate the holes; which are the following methods:

- Increasing thermal energy – if temperature of n-type Si is increased, holes are generated in small numbers due to covalent bond breaking by thermal energy supplied.

- Applying Breakdown field – if anodic bias is increased till n-type Si breakdown field strength ($3x10^5$ V/cm) is reached, large currents start flowing through the circuit. These

currents are due to avalanche multiplication causing Si dissolution. For Si with sharp pore tips, a lower anodic bias can create a field equivalent to $3x10^5$ V/cm (Lehmann 1993).

- Including oxidizers in electrolyte – Strong oxidants like H_2O_2 in combination with HF can lead to porous Si formation in n-type Si (Bao, Jiao et al. 2007; Bao, Jiao et al. 2007). High anodic bias of 12-100 V is applied to initiate the etching process and obtain reasonable number of pores. Macropores obtained via this technique, showed no sidewall porosity at wall thickness less than twice depletion region width. Also, while using oxidizers, pore surface is covered with thin microporous layer. Similar, microporous layer is observed in our results obtained via photoelectrochemical etching with no oxidizer. Etch rate achieved via addition of oxidizers is around 30 µm/min (extremely high) (Bao, Jiao et al. 2007).

- Diffusing p-type impurity at backside of high resistivity n-type Si – p+ layer with a dopant concentration, in the range of $2x10^{20}/cm^3$ is diffused at the backside of n-type Si. This process creates a p-n junction at the backside of Si. Holes generated due to p-type impurity, diffuse through the n-type bulk and reach silicon-electrolyte interface on application of an anodic bias. Etch rates obtained by this process range from 0.275 to 0.425 µm for a resistivity of 3.8-5.5 kΩ-cm n-type Si. Anisotropy is achieved due to sidewall passivation by depletion region. In low resistivity n-type Si lifetime of charge carriers in bulk silicon is reduced by high temperature processes such as diffusion, ion implantation and further annealing, limiting this technique to higher resistivities (Badel, Linnros et al. 2003).

- Applying magnetic field – High aspect ratio porous Si can be obtained on n-type Si without illumination by applying magnetic field. In Hall-effect assistance technique an inversion layer is created at silicon-electrolyte interface by Lorentz force due to which holes essential

for electrolytic dissolution are created. Grouped wire like structures instead of rigid macroporous structures are obtained by this technique (Lin, Tsai et al. 2007).

- Illumination – Photons from incident light when absorbed create holes in Si. The criterion for photon absorption is photon energy of the incident light must be greater than or equal to band gap of Si (1.12eV).

$$E = h.c/\lambda \quad (2.3)$$

Light with wavelength less than 1.1 µm (From Equation 2.3) is suitable for creating minority charge carriers (holes) in n-type silicon. Porous Si thin films are produced by irradiation with UV, visible, or infrared lasers on n-type Si using HF solution. This technique is named photoelectrochemical etching of Si even though Si is not connected to external power supply and the electric field is due to band bending. Term 'electrochemical' is used to indicate a charge transfer based chemical dissolution, while the term 'photo' means the process initiated by irradiation with laser. Porous Si films are obtained at 0.5-5 W/cm^2 laser fluencies. On dissolution, a Gaussian shaped pit is obtained and the pit has two interfaces; solution/por-Si at the top and por-Si/c-Si at the bottom. Depth of the pit and porous silicon are a function of incident light intensity. At 550 mW/cm^2 and with 48% aq. HF, the pit etch rate prior to por-Si removal is approximately 0.0245 µm/min (Koker and Kolasinski 2000; Koker and Kolasinski 2001) which is less than an order of magnitude as compared to our results from external anodic bias application. Only at 1000 W/cm^2 or greater laser intensities (Argon-beam laser (514.5nm)) (Lim, Brock et al. 1992), etch rates comparable to that obtained during photoelectrochemical etching (applying external bias) are observed.

Another widely studied technique for etching n-type Si is wet photoelectrochemical etching of Si where an external bias is applied to induce electrochemical etching and a light source (photon

energy > band gap) forms the minority charge carrier (hole) generation source. Holes can be

created from backside of silicon-electrolyte interface or frontside that is at the silicon-electrolyte

interface. These two techniques will be discussed in detail under sections 2.7 and 2.8.

2.6 Charge Transfer Mechanisms

The charge transfer mechanisms in Si are diffusion, drift and tunneling. Dominance of each

component depends on the resistivity (dopant concentration) of Si.

Diffusion currents arise due to concentration gradient of holes. Diffusion is the dominant pore

formation mechanism at high resistivities (Lehmann 1993).

Drift occurs when mean free path of holes exceeds depletion region width, holes with sufficient

energy can traverse potential barrier and cross the depletion region. For high dopant densities ($>$

10^{16}/cm^3 obtained experimentally), the depletion region width drastically reduces. Thus, instead

of diffusion, drift dominates the charge transfer. In this case, although the depletion region width

might differ in pits and planar regions, current remains same everywhere and consequently, no

pore formation is seen. Charge carrier drift gives rise to isotropic etching process (Lehmann

1993).

Tunneling occurs at very high dopant densities ($>10^{18}$/cm^3). It is dependent on depletion region

width which is in nanometer range and, mesoporous layer is obtained on the surface (Lehmann

1993). Therefore, macropore formation is not expected with highly doped Si.

2.7 Wet Photoelectrochemical Etching Using Backside Illumination

From band bending diagram Figure 2.1, n-type Si is under depletion during anodization. In n-

type Si holes are minority charge carriers, at equilibrium, the hole concentration is lower than

electron concentration. On illumination ionized n-type dopants, electrons and holes form the

three types of charges in n-type Si. In the bulk, holes recombine with the electrons and charge

17
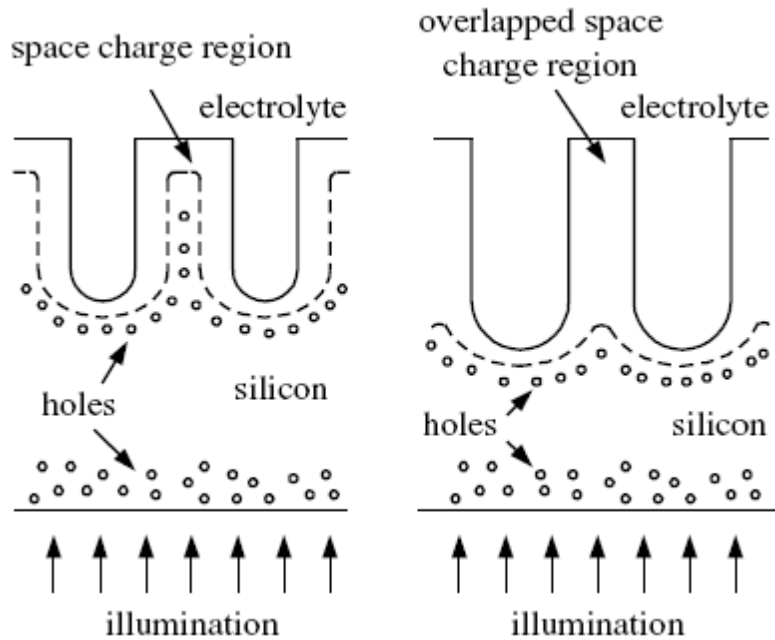
Figure 2.6. Macropore formation with back side illumination abiding Depletion Region model. Reference Tao et al., "Macroporous silicon-based deep anisotropic etching" J. Micromech. Microeng. 15 (2005) 764-770. (Reprinted with permission from IOP Science.)

neutrality occurs. Recombination is a function of the hole diffusion length. Hence, Lehmann et al believe depletion region is not the cause of passivating pore walls of n-type Si, instead the hole diffusion length forms a major factor for passivating the pore walls during backside illumination (Lehmann and Ronnebeck 1999). Contrary to the above theory, several researchers have observed formation of sidewall pores as wall thickness exceeds twice the depletion region width (Tao and Esashi 2005; Astrova and Fedulova 2009; Guozheng, Shencheng et al. 2010). This was in agreement with the theory proposed by space-charge model. According to this model, n-type silicon-electrolyte interface is similar to p-n one-sided step junction. Large potential drop is observed across the depletion region. As reverse bias voltage is reduced, depletion width decreases leading to increased hole diffusion in between the pore walls (Figure 2.6). Relation between the depletion region width and the applied bias is expressed as follows:

$$W_{DR} = \sqrt{\frac{2.\varepsilon_0.\varepsilon_{Si}.V_{eff}}{q.N_D}} \qquad (2.4)$$

$$\text{Where, } V_{eff} = V_{bi} - V_{app} \qquad (2.5)$$

where, W_{DR} is the depletion region width, ε_0 is the permittivity of free space, ε_{Si} is relative permittivity of Si, V_{bi} is the built-in potential of Si, V_{app} is the applied potential, q is the elementary charge, N_D is the donor concentration, k is the Boltzmann's constant, T is the temperature in Kelvin and n_i is the intrinsic concentration (Wehrspohn, Schweizer et al. 2007).

n-type patterned Si (100) substrates having a resistivity of 5-15 Ω-cm are photoelectrochemically etched with HF using backside illumination to obtain macropores. Non-porous sidewalls are
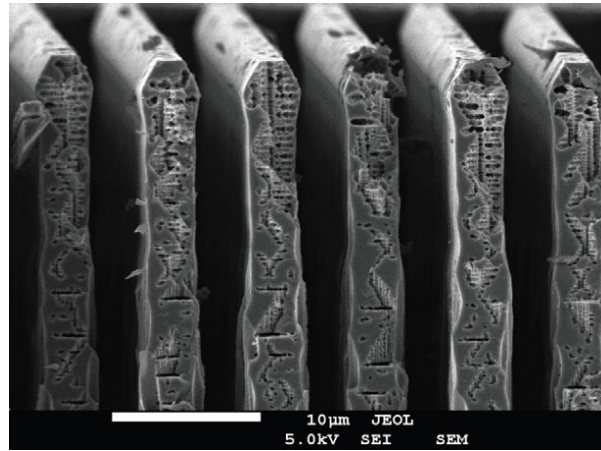
Figure 2.7. n-type Si (100) 5-15 Ω-cm with wall thickness ~ 4µm showing microporous walls. Reference Astrova et al., "Formation of deep periodic trenches in photo-electrochemical etching of n-type silicon" J. Micromech. Microeng. 19 (2009) 095009 (11pp). (Reprinted with permission from IOP Science.)

obtained based on pitch and the current density and it is established that the average distance between pores in a row depends on the period of seed grooves (patterned area etched chemically with KOH), current density and Si resistivity.

Also, to obtain smooth sidewalls an approximate relationship between pitch and silicon resistivity (ρ) was deduced:

$$\text{Average distance between macropores (µm)} \sim 2\sqrt{\rho(\Omega - cm)} \qquad (2.6)$$

Smooth sidewalls are obtained when distance between macropores of patterned array is close to the average distance between self organized macropore array (Astrova and Fedulova 2009). Growth of pores on n-type Si with different resistivities and potential can be observed from Figure 2.8 from where it is concluded real distance between adjacent pores on an unpatterned substrate did not always adhere to the space-charge model (Al Rifai, Christophersen et al. 2000). Space-charge model suggested average distance between the adjacent pores is twice depletion
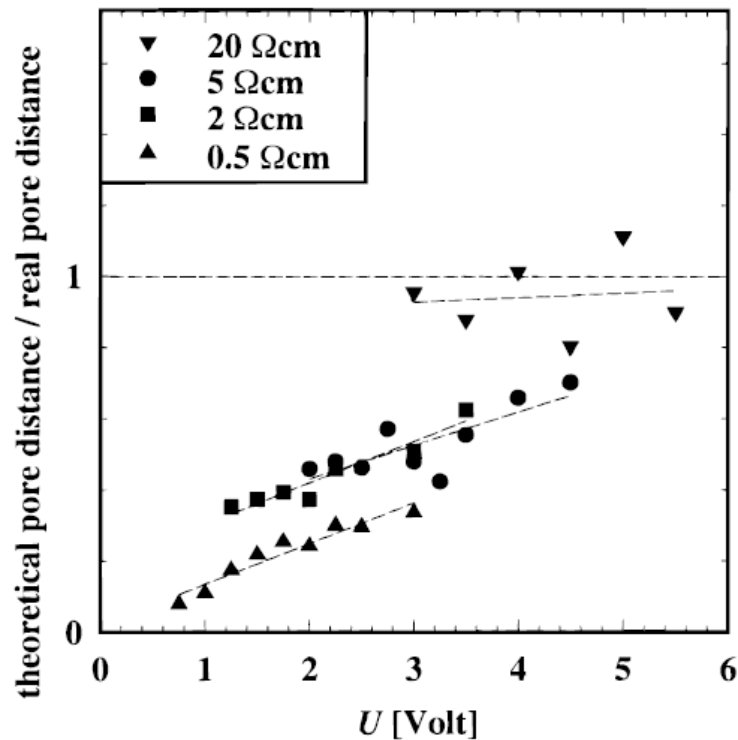
Figure 2.8. Pore distance vs. etching potential normalized to the space-charge model. Reference Al Rifai et al., "Dependence of macropore formation in n-Si on Potential, Temperature and Doping", Journal of The Electrochemical Society, 147 (2) 627-635 (2000). ("Reproduced by permission of The Electrochemical Society.")

region width. Substrates with low dopant concentration (resistivities greater than 5 Ω-cm) showed results consistent with the space-charge model; however, for samples with low resistivity or low applied bias, wall thickness between the adjacent macropores is more than predicted by

the space-charge model (Al Rifai, Christophersen et al. 2000). Our work focuses on 10-20 Ω-cm n-type Si for use in microelectronics; therefore, macropore formation would be in agreement with the space-charge model, for hole generation by backside illumination.

The depletion region formed at electrode-electrolyte interface is depleted of mobile charge carriers leaving behind immobile donor ions. On application of an external bias, there is a change in the gap between Si Fermi energy and electrolyte chemical potential. Therefore, the depletion region width varies with the applied bias. Pore geometry also has an effect on the depletion region. For a conical pore, the depletion region width is less than for planar surface and this width is minimum at the pore tip. Under forward bias and under no bias there are few holes in the depletion region. On applying a reverse bias, holes tend to diffuse from higher concentration (bulk) region to lower concentration region and give rise to diffusion current.

Several researchers have created 100-500 μm deep macropores in n-type Si(100) via photoelectrochemical etching by generating minority charge carriers using backside illumination (Lehmann and Foll 1990; W., J. et al. 1995; Barillaro, Nannini et al. 2002; Barillaro, Bruschi et al. 2005; Tao and Esashi 2005; Kim, Kim et al. 2006; Guozheng, Shencheng et al. 2008; Astrova and Fedulova 2009; Li, Seo et al. 2009; Zhao, Guo et al. 2010). Barillaro et al. demonstrated structures ranging from vertical vias, trenches, spirals and other complicated patterns on n-type Si with resistivity 2.4-4 Ω-cm by selecting appropriate seed (mask) for photoelectrochemical etching. The structures formed showed sidewall etching for variations in pitch, seed diameter and Si resistivity. (Lehmann and Foll 1990; Barillaro, Nannini et al. 2002; Barillaro, Bruschi et al. 2005; Tao and Esashi 2005; Astrova and Fedulova 2009). Astrova et al formulated an approximate relationship (Equation 2.6) between the pitch and Si resistivity. This formulation

was based on the pitch obtained with self organized macropores. Equation 2.6 is useful to select an appropriate mask in order to create anisotropic structures (Astrova and Fedulova 2009).

Understanding constraints for fabricating macropores at isolated locations in Si, microstructures are obtained in low doped silicon (100) (>1 Ω-cm) by creating macroporous Si using backside illumination followed by chemically dissolving the macroporous Si in Tetramethylammonium hydroxide (TMAH). Tao et al. observed sidewall etching at corner rows of patterned array to be more pronounced at high applied bias and low resistivity substrates. 50µm and 175 µm lateral overetch is reported at 2V for 1000 Ω-cm and 5-8 Ω-cm, respectively (Tao and Esashi 2005). Although, 300 µm deep microstructures with vertical walls are fabricated, these structures had large opening diameter (> 100 µm).

Thus, operating at sidewall thickness greater than depletion region width leads to sidewall etching and poses a challenge to obtain isolated, high aspect ratio microstructures.

2.8 Wet Photoelectrochemical Etching Using Frontside Illumination

Frontside illumination means to illuminate silicon-electrolyte interface; to create minority charge carriers at the Si surface in contact with the electrolyte.

Lehmann and Foll demonstrated Si dissolution with no external bias using both frontside and backside illumination of blank n-type silicon. They believe, during front side illumination charge carriers are generated near the surface whereas backside illumination gives rise to charge carriers in bulk. Depth of the trench is promoted only when the charge carriers are present in the bulk while near-surface charge carriers lead to lateral expansion of the trenches. And hence, back side illumination is preferred over front side illumination for creation of deep trenches (Lehmann and Foll 1990). While this argument is valid for tight pitches, we run into the problem of sidewall etching as we work with patterns that are located at a wall thickness much greater than twice the

depletion region width. When patterns to be etched have wall thickness greater than twice the depletion region width, presence of holes in bulk silicon will lead to sidewall etching (porous sidewalls). Frontside illumination might work to create isolated anisotropic microstructures since the holes are generated near silicon-electrolyte surface. Conical TSVs are obtained in frontside illumination, since vertical etch rate is more than lateral expansion rate.

During photoelectrochemical etching with frontside illumination, two layers of porous Si are obtained. The top layer consists of porous Si film (Levyclement, Lagoubi et al. 1993; Levyclement, Lagoubi et al. 1994). This film shows a tangled network of Si wire like structures. It is observed that this microporous or nanoporous layer has structures of various sizes and it varies from amorphous to crystalline silicon in the same layer. Amorphous-like porous structure may be generated due to diffusion current by photo-carriers generated beyond depletion layer (Arita 1978). Our results with lower wavelength photon source are in agreement with the theory by Arita. Explanation to the formation of microporous crystalline silicon is based on the residual stress (Levyclement, Lagoubi et al. 1994). It is suggested macroporous silicon shattered into fine filaments due to the residual stress. The pattern of shattered structure is analogous to a comb-like structure where the teeth are separated by an oxide layer. -Si-Si- bonds form the filament and -Si-O- bonds form the gap in contact with the electrolyte (Galun, Tenne et al. 1993; Levyclement, Lagoubi et al. 1994). Underneath the nanoporous or microporous layer, a macroporous layer formed out of micron sized pores is observed. Work by Levy clement et al. on low doped ($N_d = 10^{15}$/cm^3) n-type Si shows total etch pit depth as well as the nanoporous and macroporous layer depth to increase with an increased applied charge density (Levyclement, Lagoubi et al. 1994). During photoelectrochemical etching with frontside illumination the total depth of the etch pit increases with anodization time. With frontside illumination using a 50 W Tungsten-Halogen

23

lamp, and HF/ethanol as electrolyte on 1-3 Ω-cm Si, pore diameter increases with anodization time. Dissolution in lateral direction along with an etch in principal axial direction is viewed; although maximum etch rate is in the axial <100> direction. Presence of a dihydride Si surface at KOH pit bottom causes steric hindrance, leading to a higher stress at the bottom of KOH pit (Outemzabet, Gabouze et al. 2005). Hence, chemical reactivity is more at the KOH pit bottom in the <100> direction. Lateral expansion is attributed to photon absorption at sidewalls during frontside illumination. Lateral etching is maximum at the pore top and adjacent pores tend to merge with time convincing that the sidewalls are not passivated by depletion region during photoelectrochemical etching with frontside illumination. Pore propagation rate into bulk is
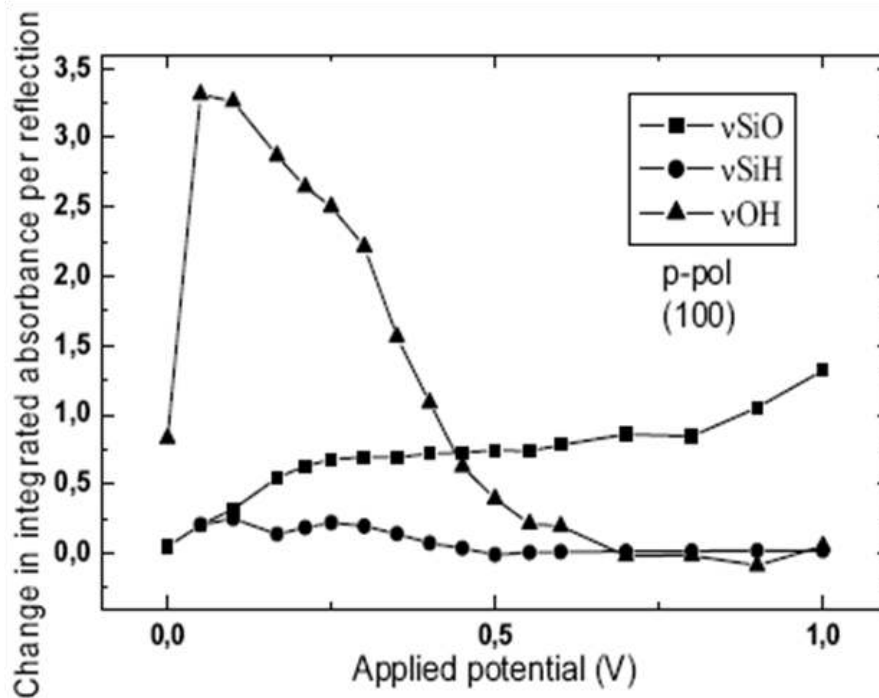
Figure 2.9. Integrated infrared absorption as a function of applied potential for p-type Si (100). Reference Outemzabet et al., "Random macropore formation in n-type silicon under front side illumination: correlation with anisotropic etching", Phys. Stat. Sol. (c) 2, No. 9, 3394–3398 (2005). Copyright Wiley-VCH Verlag GmbH & Co. KGaA. Reproduced with permission.

slower than backside illumination, since, the holes generated close to the surface induce lateral etching and do not contribute towards vertical dissolution.

Researchers have proved n-type and p-type Si different in their electronic property, nevertheless, their chemistry remains similar (Gerischer and Lubke 1987; Lehmann 1993). Figure 2.9 shows infrared absorption as a function of applied potential on p-type Si (100) illustrating dominance of -OH bonds at low anodic as compared to Si-H and Si-O bonds. Si-O bonds increase as with increasing potential. Presence of an oxide layer promotes local reactivity at kink sites (Gerischer and Lubke 1987). Hence, at high applied bias, more nucleation sites are observed because of excessive hole concentration leading to dissolution in different directions. It is found macropore growth in <100> direction becomes constant once the nucleation period is over, however the diameter of the pores increases with time (Outemzabet, Gabouze et al. 2005).

2.9 Electrolyte Selection

The criterion for the electrolyte selection is primarily based on achieving a higher etch rate. Mixtures of HF with other solvents form the electrolyte for Si wet electrochemical etching. Although the electrolyte composition is not specifically created for sidewall passivation, it plays a major role in increasing the overall Si dissolution rate (Lehmann and Ronnebeck 1999). Electrolytes used in Si anodization can be classified into several categories such as aqueous, organic and ionic.

Aqueous electrolytes are mixtures of HF and water, but can also contain fluorine containing salts (tetrafluoroborate) (Flake, Rieger et al. 1999), organic alcohol additives such as ethyl alcohol, (Barillaro, Bruschi et al. 2005; Li, Seo et al. 2009) and Isopropyl alcohol (Bhattacharya, Rani et al. 2005; Harraz, Kamada et al. 2005), pH adjusters (Ammonium fluoride), and surface tension reducing agents (Triton X-100, Mirasol). Surfactants help remove the H_2 bubbles off the pore

25

walls and improve HF contact with Si surface, thereby increasing the etch rate (Lehmann and Foll 1990; W., J. et al. 1995; Guozheng, Shencheng et al. 2010).

Organic electrolytes contain organic solvents such as Acetonitrile (Flake, Rieger et al. 1999), Dimethylformamide, Dimethylsulfoxide mixed with HF and water (Lust and Levy-Clement 2002).

Room temperature ionic liquids such as 1-ethyl-3-methylimidazolium $EMIm(FH)_{2.3}F$ with high conductivity form the fluoride source to create porous Si (Raz, Shmueli et al. 2010).

Kim et al. observed that sidewall porosity is a strong function of depletion region width and different additives and electrolytes show no effect in passivating the sidewalls. However, electrolyte composition has a strong impact on the etch rate (Kim, Kim et al. 2006).

2.10 Overetching

Overetching at macropore array edge prohibits an exact translation of etch mask onto Si during wet electrochemical etching. Figure 2.10 illustrates overetching due to excess stress, carrier transport, and sidewall branching. Stress induced overetching results in small depth macropore
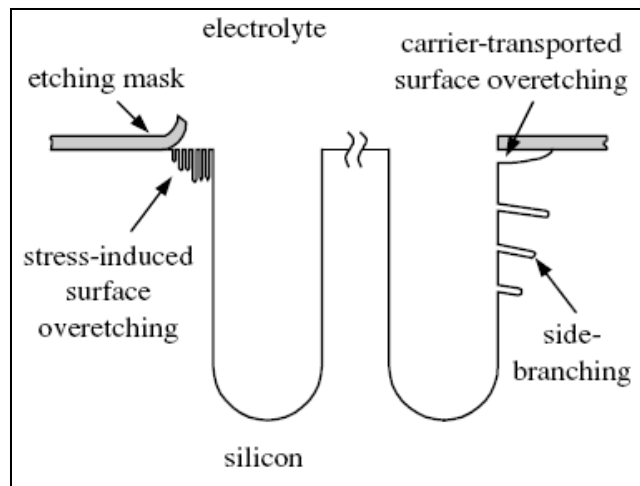
Figure 2.10. Overetching at macropore array edge. Reference Tao et al., "Macroporous silicon-based deep anisotropic etching" J. Micromech. Microeng. 15 (2005) 764-770. (Reprinted with permission from IOP Science.)

formation at the corner of the patterned area because of preferential carrier concentration at stressed regions. Transport of carriers from the bulk to the masked area leads to carrier transport based and sidewall branching based overetching (Tao and Esashi 2005). Stress induced overetching is observed at every opening in the patterned area during front side illumination.

2.11 Wavelength of Irradiation Source

During wet photoelectrochemical etching of n-type Si, light source irradiating the Si surface must possess a photon energy equivalent or greater than band gap energy of Si. Si can absorb photons with wavelengths less than 1108 nm (Equation 2.3). The photon absorption depth in Si is a function of the incident photon energy. Higher wavelength light is absorbed deeper in Si as compared to lower wavelength light. Thus, it is feasible to create minority charge carriers (holes) within the depletion region of Si as well as beyond the depletion region width. When light with higher wavelengths were used in combination with backside illumination, the penetration depth in Si being higher or of the same magnitude as that of the thickness of the wafer, holes are induced in the frontal surface at the silicon-electrolyte interface. Holes formed at the silicon-electrolyte interface create trenches covered with porous silicon (Guozheng, Shencheng et al. 2008).

3 MATERIALS AND EXPERIMENTAL PROCEDURE

3.1 Substrate Preparation

Blank n-type (phosphorus doped) silicon (100) wafers (n-type Si) were obtained from Montco Silicon Technologies, CA. n-type Si wafers were deposited with 1 micron thick low stress silicon nitride by LPCVD process at Microelectronics Research Center in Georgia Institute of Technology. 20 nm Chromium and 50 nm Gold layer were deposited on silicon nitride via e-beam evaporation technique (Temescal BJD-1800 E-Beam Deposition System) at Center for Advanced Microstructures and Devices (CAMD). Gold serves in blocking the incident light from entering silicon in undesired locations. Chromium is an adhesion promoter between silicon nitride and gold. Photolithography and subsequent developing steps including Reactive Ion Etching (RIE) were performed at CAMD. Photolithography was used to pattern the Si wafers with desired pitch and pattern area. Photoresist SC-1827 (positive photoresist) was spin coated

Figure 3.1. Patterned substrate for subsequent photo-electrochemical etching.

on Cr-Au deposited 4" Si wafers using spin coater (Headway Research PWM101 Light Duty Photoresist Spinner). Photoresist was soft baked at 90°C for 30 minutes and then exposed to 100 mW/cm^2 UV light for 15 seconds with an appropriate photomask using Lithography tool (Oriel UV Exposure Station with Aligner). During development, Cr was removed by Chrome etchant, gold was dissolved using gold etchant, and the exposed photoresist was dissolved in 351

developer. On developing, the wafer was hard baked at 90ºC for 30 minutes and silicon nitride was etched using Reactive Ion etching technique (Oxford PlasmaLab 100 ICP-DRIE System). Remnant photoresist was dissolved in acetone. Inverted pyramidal pits were created by chemically etching exposed Si with 86.2 volume% Potassium Hydroxide solution (30%) (KOH, Fischer Scientific, USA) and 13.8 volume% Isopropyl alcohol (IPA (ACS grade), Mallinckrodt Baker, USA). KOH was initially heated to 70°C followed by IPA addition, on attaining 70°C Si substrates were immersed completely in the solution and the temperature was maintained between 70- 77°C for 4-10 minutes depending on the area to be etched. KOH etched wafers were further subjected to photoelectrochemical etching. (Note: For the experiments with p-type Si (Boron doped) (Montco Silicon Technologies, CA), metal layers (chromium and gold) are not necessary and illumination source is not required)
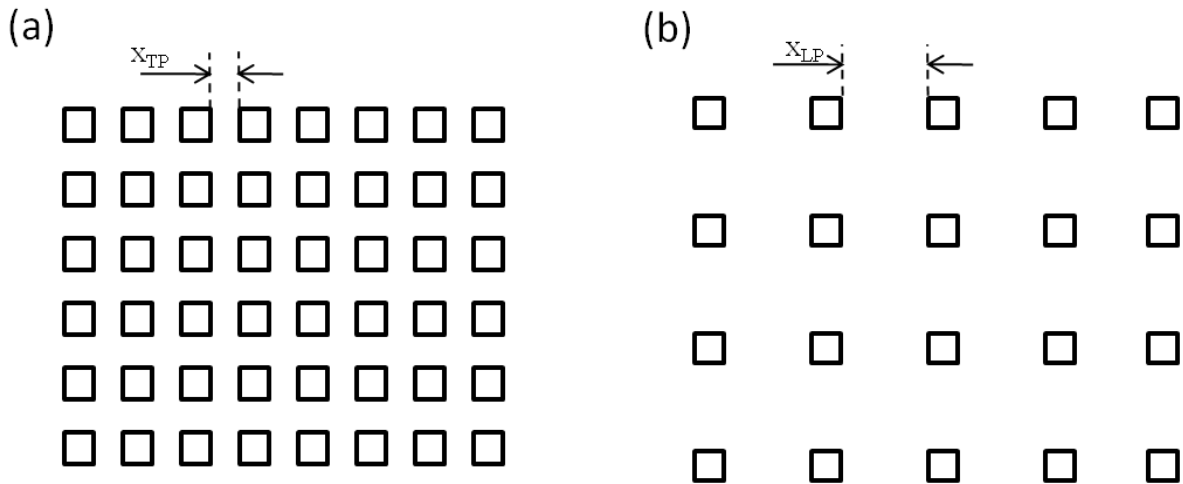
Figure 3.2. Pattern created by Lithography; (a) dense, (b) isolated.

Dense and isolated patterns can be created on Si using lithography. In the Figure 3.2, x_{TP} and x_{LP} are the wall thickness of tightly pitched and loosely pitched structures, respectively. The wall thickness is classified as tightly pitched or loosely pitched relative to the depletion region width (W_{DR}); $x_{TP} \leq 2.W_{DR}$ (dense pattern – Figure 3.2a) and $x_{LP} > W_{DR}$ (isolated pattern – Figure 3.2b).

3.2 Photoelectrochemical Etching Experimental Set-up

Si substrate was dipped in ethyl alcohol (Fischer Scientific, USA) for 1- 2 minutes and rinsed with DI water. This was succeeded by a 10% Hydrofluoric acid (HF, Sigma Aldrich, USA) dip to remove the native oxide followed by rinsing with water and drying in air. Schematic for
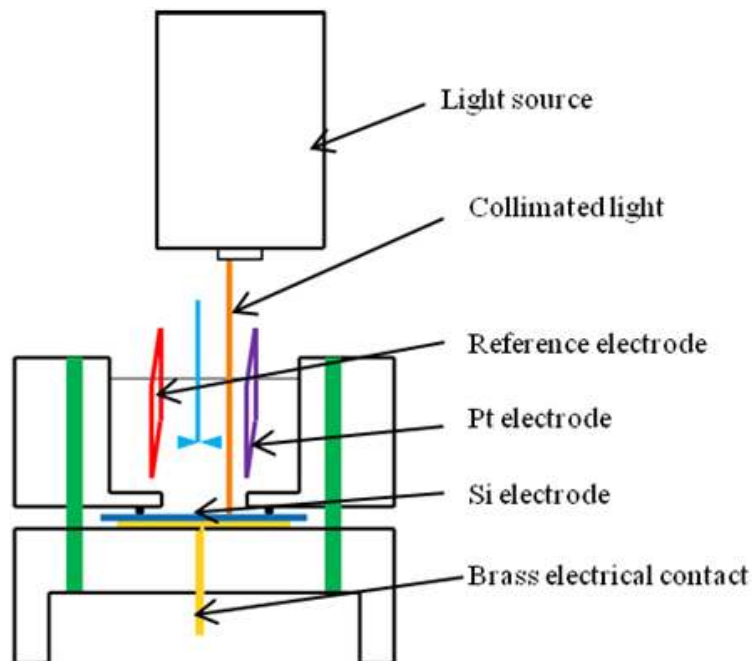
Figure 3.3. 2D schematic of a photo-electrochemical cell.

photoelectrochemical etching is depicted by Figure 3.3. The reactor used for electrochemical etching was made of Teflon and has a brass electrode at the bottom to provide electrical contact. Gallium-Indium eutectic was applied evenly on the brass electrode to achieve good electrical contact between Si (anode) and the brass electrode. Once the substrate (working electrode) is placed, the reactor was sealed with an o-ring. Platinum counter (cathode), platinum pseudo reference and the working electrode were connected to potentiostat (Princeton Applied Research Potentiostat/Galvanostat Model 263A). Figure 3.4a shows the laboratory set-up of the electrochemical cell.

HF in combination with aqueous and/or organic solvents formed the etching electrolyte. Aqueous electrolyte containing 5.21M HF, 48.15% (vol) Isopropyl alcohol (IPA), and 1480 ppm Triton X-100 formed the typical electrolyte composition (BKM) used in most etching
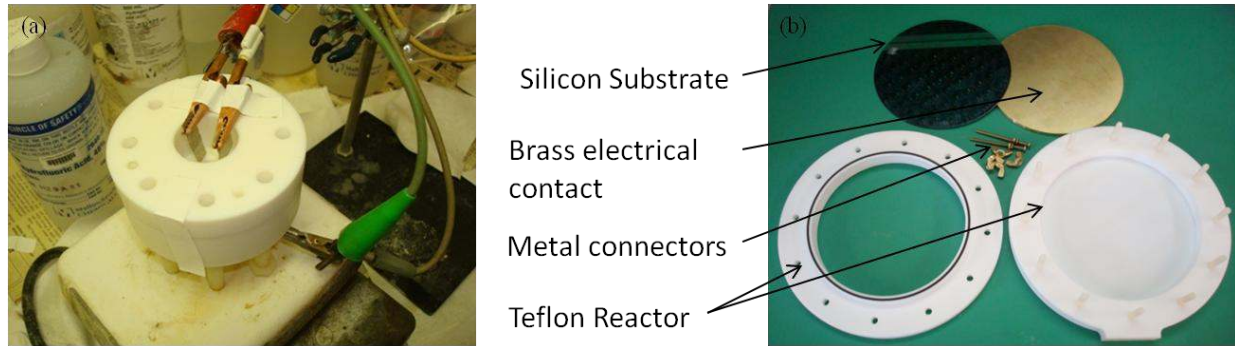
Figure 3.4. Electrochemical cell (a) assembled with electrode connections, and (b) disassembled.

experiments unless otherwise mentioned. The electrolyte composition is obtained from literature (Kim, Kim et al. 2008) and was further optimized to achieve high etch rates. Etching experiments were performed using potentiostat in the chronoamperometry mode, by keeping the applied potential constant vs. pseudo reference electrode. n-type Si is photoelectrochemically etched using a collimated light source. In our experiments, red light (632.8 nm) from HeNe laser (CVI Melles Griot, USA) with a maximum average light intensity of 461.11 mW/cm^2, and blue light (365 nm) from an UV LED (M365L2-C4, Thorlabs, USA) with an average light intensity of 7.8 mW/cm^2 were used. In order to control and reduce the light intensity from the HeNe laser neutral density filters (Thorlabs, USA) were used.

3.3 Methods for Analysis

The patterns on Si are ≥ 6 μm in width, but the sidewall porosity is in the nm range and hence, for a detailed structural and morphological analysis Scanning Electron Microscope (FEI Quanta 3D FEG Dual Beam SEM/FIB) was used. The cross-section of the microstructures etched in Si

were observed by manually cleaving the Si samples with a scriber. Samples were placed vertically in the SEM to measure the depth attained. The imaging process is simple and quick with SEM.

The size of the structures being in the micron range, it is a challenge to manually cleave the substrate at the preferred location. Focus Ion Beam - Scanning Electron Microscope (FEI Quanta 3D FEG Dual Beam SEM/FIB) is a tool that mills the substrate at the desired location using an Ion beam. Samples were back filled with an epoxy M bond 610 (Ted Pella Inc., USA) and sputtered with gold using a sputter coater prior to analysis using FIB-SEM. FIB-SEM technique is time consuming for micron sized structures. Hence, most of our analysis is done using SEM by manually cleaving the wafers.

4   RESULTS AND DISCUSSION

4.1 Frontside Versus Backside Illumination

Photoelectrochemical etching of n-type silicon (Si) is carried out by illuminating the Si surface with light possesing photon energy greater than the band gap of Si (1.12 eV). Minority Chrage carriers (holes) are formed in n-type Si on photon absorption. The morphology of porous Si is a strong function of illumination method (backside or frontside).
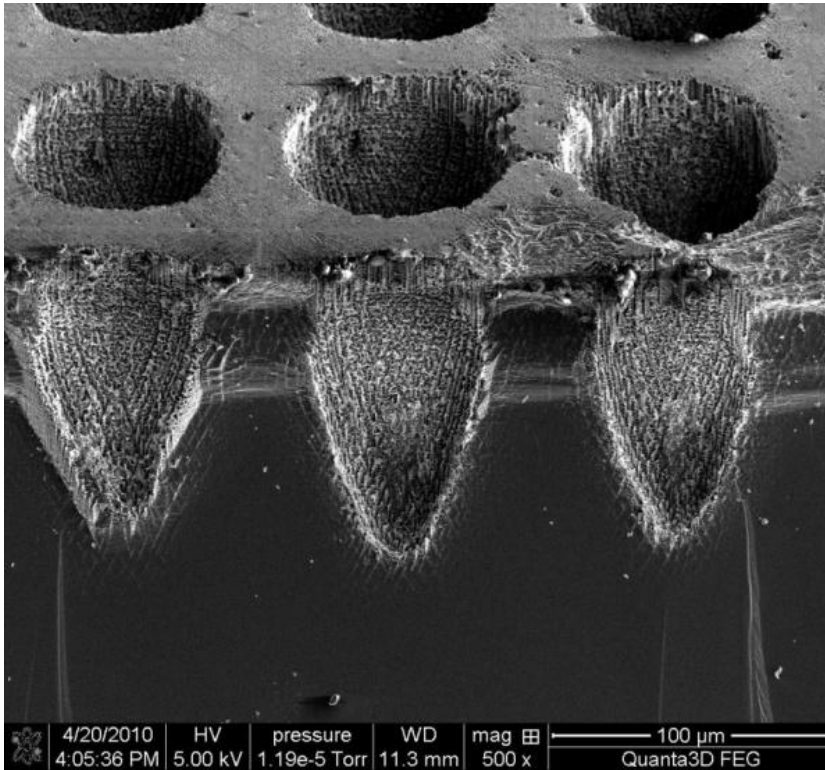
Figure 4.1. n-type Si (100) 10-20 Ω-cm, pitch =100 µm, starting diameter =30 µm, average light intensity = 46.11 mW/cm2, final depth = 100 µm, etch rate = 1.49 µm/min.

In this work, frontside illumination is used for wet photoelectrochemical etching of Si. Patterned n-type Si (10-20 ohm-cm) is photoelectrochemically etched in an aqueous electrolyte containing 5.21M hydrofluoric acid (HF), 48.15% (vol) isopropyl alcohol (IPA), and 1480 ppm Triton X-100 (BKM electrolyte). Si is anodically biased at 5 V versus Platinum (Pt) pseudo reference

electrode. An average light intensity of 46.11 mW/cm^2 from a HeNe laser (632.8 nm) is used to irradiate silicon-electrolyte interface. Deep microstructures with 100 µm depth and 78 µm width are obtained. Inverted pyramidal shaped pits created in the patterned regions by chemical dissolution using potassium hydroxide (KOH) solution, act as etch seeds for further photoelectrochemical etching. The depth and width of the etch seeds vary with the pattern opening and the duration of chemical dissolution. Figure 4.1 shows the SEM image of deep microstructures created using photoelectrochemical etching with 30 µm wide 10.6 µm deep KOH pits. On photoelectrochemical etching a vertical etch rate of 1.49 µm/min and a lateral etch rate of 0.4 µm/min are obtained leading to anisotropy of 0.73 (Anisotropy $= 1 - \frac{\text{lateral etch rate}}{\text{vertical etch rate}}$). The microstructure walls make an angle of 70-80º with horizontal Si (100) crystal plane. The microstructures are covered with a microporous tangled layer that formed the top layer and macropores existed below the microporous layer. Further, the sidewalls near the top surface show lateral etching; hence porous. Towards the microstructure bottom, the wall in-between adjacent microstructures showed no porosity. These initial results formed the basis to select frontside illumination for wet photoelectrochemical etching to create isolated, anisotropic, and deep microstrcutures in n-type Si. Astrova et al showed (Figure 2.**7**) using backside illumination on n-type Si, creation of anisotropic isolated structures with sidewall thickness greater than 9 µm and 2.3 µm for 15 Ω-cm and 5 Ω-cm, respectively, is difficult and has not been widely published.

The morphology of microstructures created using wet photoelectrochemical etching differ significantly based on the illumination technique. On illuminating the Si from backside (away from silicon-electrolyte interface), the incident photons are absorbed in the bulk (Figure 4.2a). When an anodic bias is applied to n-type Si, the holes generated in the bulk are brought to the

silicon-electrolyte interface. Hence, we believe behavior of backside illuminated n-type Si would be similar to p-type Si (majority charge carriers - holes). If the patterns are loosely pitched (wall thickness > 2 × W_{DR} (Depletion Region width)), holes are present around the microstructure leading to sidewall porosity (dissolution along more than one crytalline orientations) (Figure 4.2a). On the other hand, if the wall thickness between the adjacent structures is less than or equal to W_{DR}, then the sidewalls are depleted of holes (Figure 4.2b) and dissolution is observed only along one crystalline directon. Consequently, macropores with non-porous sidewalls are obtained via photoelectrochemical etching of tightly pitched n-type silicon using backside
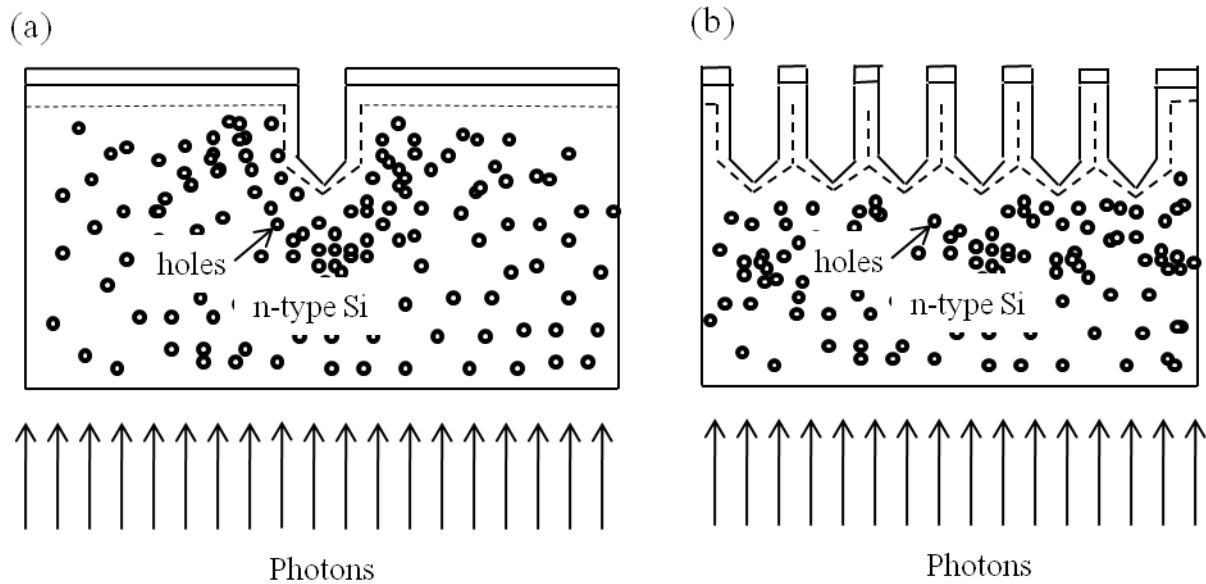
Figure 4.2. Backside illumination for patterned Si with wall thickness between adjacent structures (a) > 2 × W_{DR}, and (b) ≤ 2 × W_{DR}.

illumination. While with frontside illumination micron-sized structures can be formed at isolated locations. Frontside illumination (illumination at silicon-electrolyte interface) generates near surface minority charge carriers. Holes can be created within and beyond the depletion region width depending on absorption depth of the incident photon. Figure 4.3 shows the schematic of

hole generation using frontside illumination on n-type Si. The presence of an opaque mask (gold) helps in blocking the photons from being absorbed in the unpatterned regions.
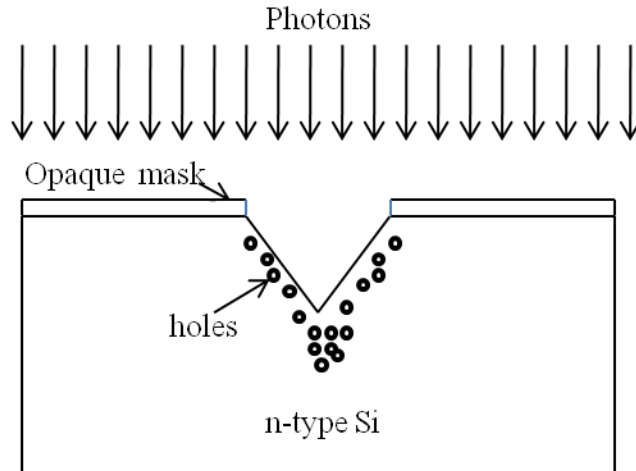
Figure 4.3. Schematic of hole generation in n-type Si with frontside illumination.

Absorption and relflection coefficients of photons not only depend on the material, and the photon energy but also on the angle of incidence (φ) of light. As shown in Figure 4.4, φ is
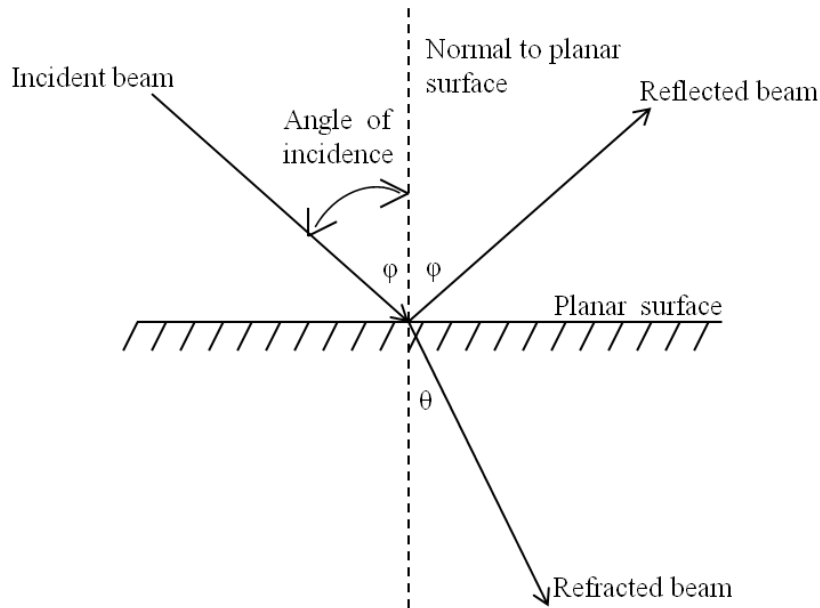
Figure 4.4. Schematic of beam of light traversing an interface between two different materials.

measured with respect to the normal to the surface. When collimated beam is used to illuminate the KOH pit or any non-planar structure, φ being different at every incidence point, the absorption and reflection coefficients will vary along the surface. For example, when collimated light is used to illuminate the KOH pit as shown in Figure 4.5, at point A φ is 54.74° while at point B, φ is 0°. As φ increases, the reflection coefficient increases thereby decreasing the photon flux absorbed. The absorbed photons generate holes in n-type Si. Also, photons from the reflected ray are absorbed as shown in Figure 4.5. Electrochemical dissolution of Si occurs in the presence of holes. During electrochemical dissolution of n-type Si, the current flowing through the circuit for a given anodic bias is goverened by the absorbed photons. Further, the electrochemical dissolution rate of Si is a function of the current flowing through the circuit. From Figure 4.1 the vertical dissolution rate is observed to be higher than the lateral dissolution rate. Hence, the current in the vertical direction is higher than the lateral direction; more photons are absorbed at the bottom of the KOH pit than the sidewalls.
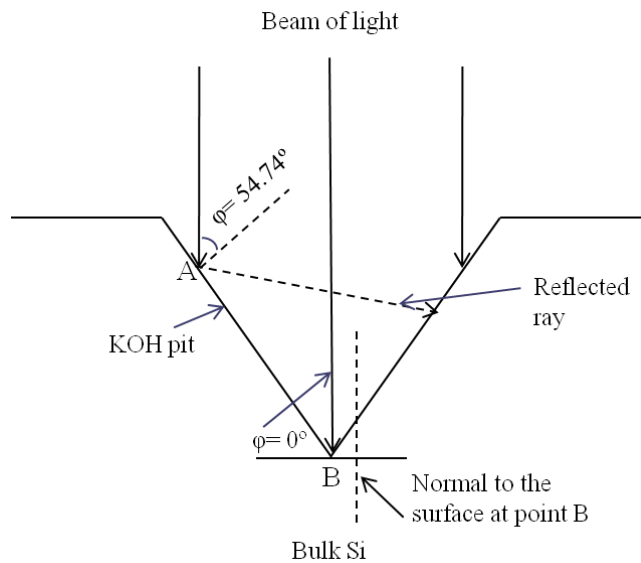
Figure 4.5. Schematic showing the angle of incidence of light at different points in a KOH pit.

While with backside illumination, a planar Si surface is illuminated. Thus, the approximate number of photons absorbed at any position remains the same. Consequently, the control over the number of holes reaching the sidewalls while working with isolated pitches is minimal.

The tendency of holes to collect at stressed regions in Si is another major factor contributing towards a higher vertical etch rate in both frontside and backside illumination. The bottom of the KOH pit is more stressed than the sidewalls; hence higher vertical etch rate observed.

The factors deciding the viability of a particular technique to create deep microstructures in Si are etch rate, anisotropy, aspect ratio, wall texture, and flexibility in creating the microstructures at any desired location.

Conditions related to etch rate and anisotropy will be discussed in section 4.1.1 to 4.1.5.

4.1.1 Etch Rate Dependence on Reaction Rate Limiting Step

Experiments with varying light intensities are performed to optimize microstructure forming conditions and to obtain operation limits. Steps governing n-type Si dissolution are based on kinetics of charge transfer and mass transfer. Etching mechanism and etched structure morphology depend on rate determining step of Si dissolution reaction. To analyze vertical etch rate variation as a function of incident light intensity, photoelectrochemical etching of blank n-type Si (10-20 ohm-cm) is carried out in BKM electrolyte for 1 hr at a potential of 5 V versus Pt. When collimated light is incident at n-type silicon-electrolyte interface, pit formation is observed. The shape of the pit is similar to the incident light intensity profile. HeNe laser has a Gaussian light intensity profile. Consequently, pit shape is Gaussian with maximum depth at center. Hence, instead of using average light intensity, the light intensity at the center of the laser beam is plotted as X-axis. The maximum depth attained by the pit is measured by manually

cleaving the wafers (for obtaining the cross-section) and observing under SEM. As seen in Figure 4.6, the etch rate is observed to increase to a certain value with the light intensity and then eventually become independent of the light intensity. At low light intensities (≤ 92.22 mW/cm^2), photon flux is lower than mass transfer rate in the electrolyte, therefore, increasing the light intensity (photon flux) leads to a corresponding increase in the etch rate. Whereas at high light intensities (≥ 230.55 mW/cm^2), the photon flux being higher, charge transfer rate becomes higher
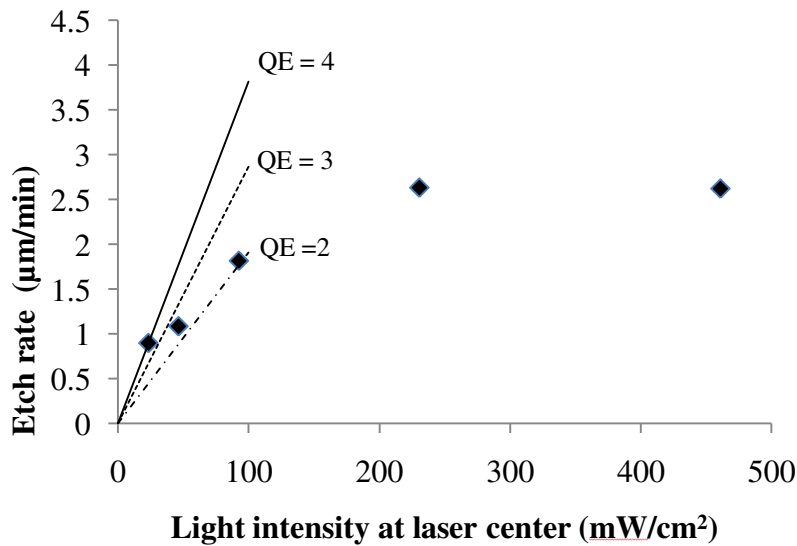
Figure 4.6. Etch rate as a function of light intensity.

than the mass transfer rate (constant in all the experiments) and thus, etch rate becomes independent of the incident light intensity. Further, the quantum efficiency, which is the number of electrons injected in the conduction band per incident photon, increases with decreasing light intensity. Quantum efficiencies of 2.0, 2.5, and 4.0 are achieved at 92.22 mW/cm^2, 46.11 mW/cm^2, and 23.05 mW/cm^2, respectively.

Figure 4.7 shows variation in vertical etch rate with agitation rate at three different light intensities (92.22 mW/cm^2, 230.55 mW/cm^2, and 461.11 mW/cm^2) on blank n-type Si (10-20 Ω-

cm) in BKM electrolyte composition. The reported light intensities are values calculated at center of HeNe laser beam. The etch rates measured correspond to the maximum depth of etch pit. At 92.22 mW/cm^2, the observed vertical etch rate remains constant with increasing stir rates, whereas at 230.55 mW/cm^2 and 461.11 mW/cm^2 the etch rate increases with increasing mass transfer rates. This shows the system becomes mass transfer limited at the higher light intensities. Once the reaction rate is limited by transport of HF, the mechanism of Si dissolution is via oxide formation. Si in the presence of water forms silicon dioxide. HF dissolves silicon dioxide isotropically which leads to electropolished surfaces. In order to obtain anisotropic
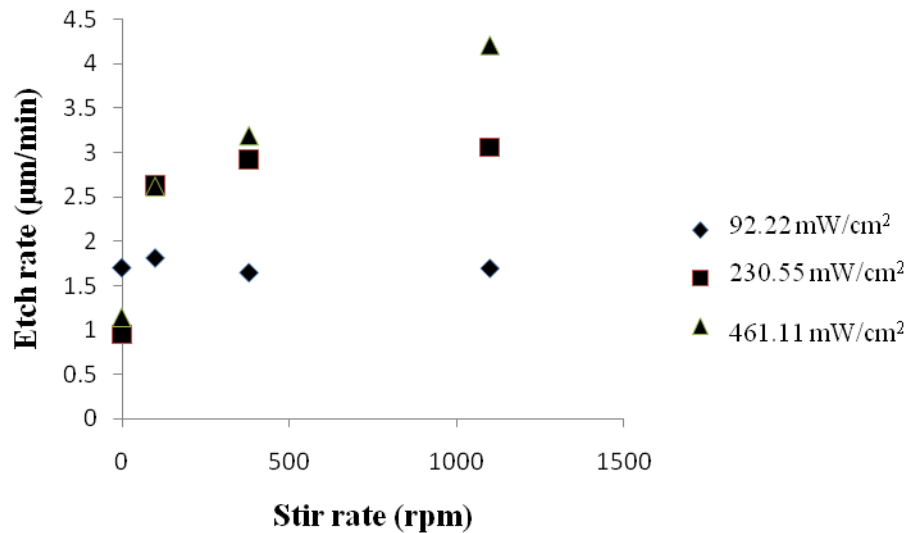
Figure 4.7. Etch rate as function of mass transfer rate.

microstructures, it is necessary to operate within kinetically limited regimes.

Thus, from Figure 4.6 and 4.7, it is found that higher etch rates can be attained at higher light intensities with no mass transfer limitations, by pushing the kinetic regime to higher light intensities using additional techniques to improve mass transfer.

4.1.2 Morphology of Etch Pit

Morphology of a pit greatly depends on the reaction rate limiting step. Unpatterned (blank) n-type Si is photoelectrochemically etched using HeNe laser (632.8 nm) to view and analyze the

morphology. HeNe laser used in all our experiments emits a beam which is Gaussian in nature and light intensity varies along the beam diameter with maximum light intensity 461.11 mW/cm^2 at the center of the beam. Hence, it is possible to expose Si to different light intensities in a single experiment allowing study on the morphology of Si in different rate limiting regimes.
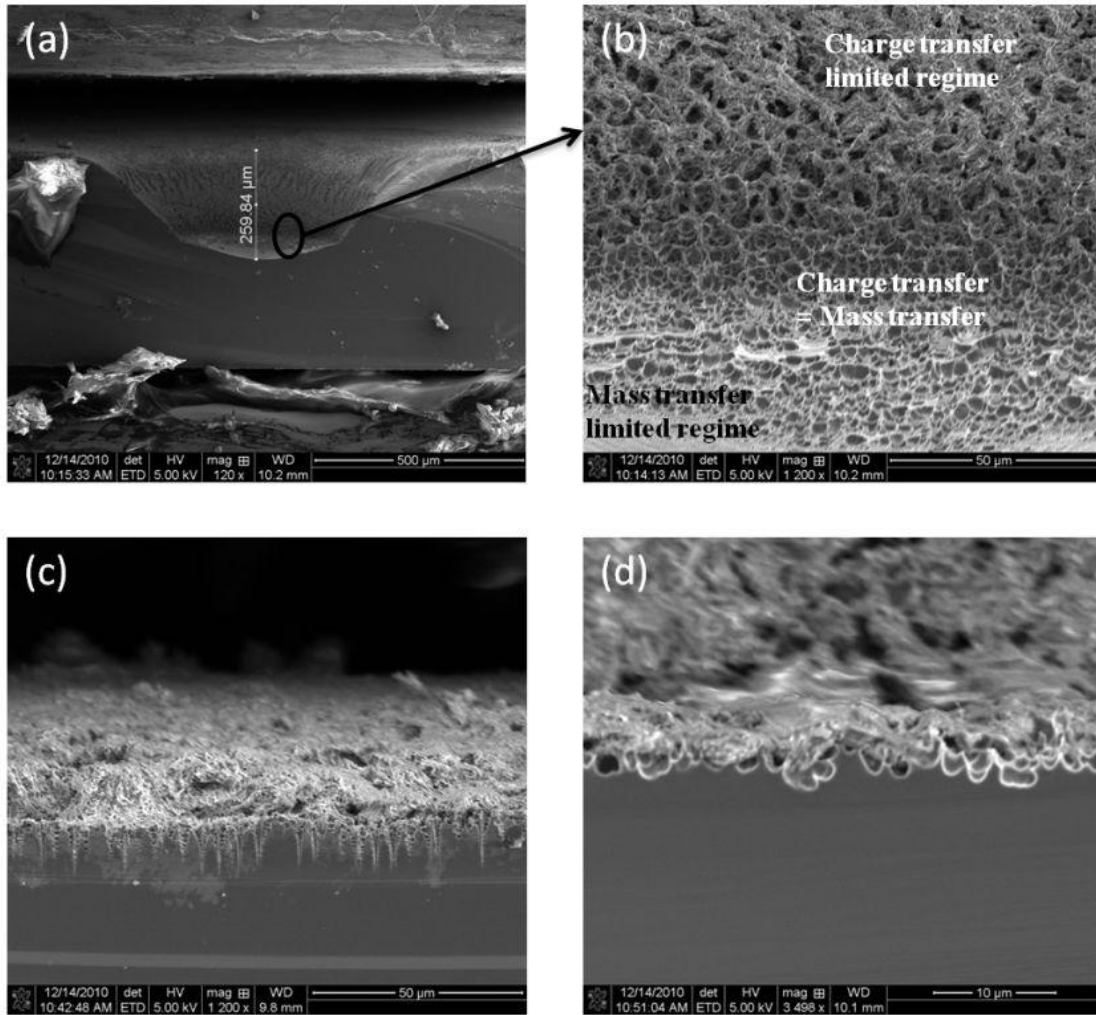
Figure 4.8. SEM image of photo-electrochemically etched blank n-type Si (10-20 ohm-cm) showing (a) cross-section of etch pit, (b) morphology at different regimes, (c) cross-section at charge transfer limited regime, and (d) cross-section at transition regime.

Figure 4.8a shows three different surface morphologies in the pit created by illuminating the sample at an average light intensity of 230.55 mW/cm^2. Figure 4.8b is a 1200x magnification showing the morphology variation with the rate limiting regime.

As seen in Figure 4.8c, in the charge transfer limited regime, macropores are formed below a microporous sheath. The depth of these macropores ranges from 2-10 µm. The overall vertical etch rate in this regime is high.

As the light intensity increases further, mass transfer rate becomes equal to charge transfer rate, shallow cup shaped pits with 2-4 µm diameters are obtained as shown in Figure 4.4d. The surface of the cup shaped structures is smooth unlike pores obtained in the charge transfer limited regime.

On further increasing photon flux, mass transfer governs dissolution rate. Mechanism of dissolution in the mass transfer limited regime involves formation of an oxide and this oxide is further etched by HF. This results in more isotropic dissolution leading to a drastic reduction in aspect ratio. Thus, the shape of the pit deviates from Gaussian profile (laser light intensity profile) during photoelectrochemical etching using high laser fluencies.

In order to obtain anisotropic pits in Si, wet electrochemical dissolution should be performed with charge transfer as the rate limiting step.

4.1.3 Effect of Light Intensity on Isolated Structures

The effect of light intensity on patterned structures is observed to determine the operating range for photoelectrochemical dissolution of n-type Si (100) (10-20 Ω-cm). Patterned Si is photoelectrochemically etched at three different light intensities 92.22 mW/cm^2, 230.55 mW/cm^2, and 461.11 mW/cm^2. Cross-sectional SEM images of the resultant microstructures are shown in Figure 4.9. At 230.55 mW/cm^2, experiments with blank Si yield electropolished surface (Figure 4.6). When patterned Si is subjected to the same light intensity, microstructures with macropores along walls covered with microporous Si is observed from Figure 4.9b. On blank Si mass transfer limited regime is attained at 230.55 mW/cm^2, whereas reaction on
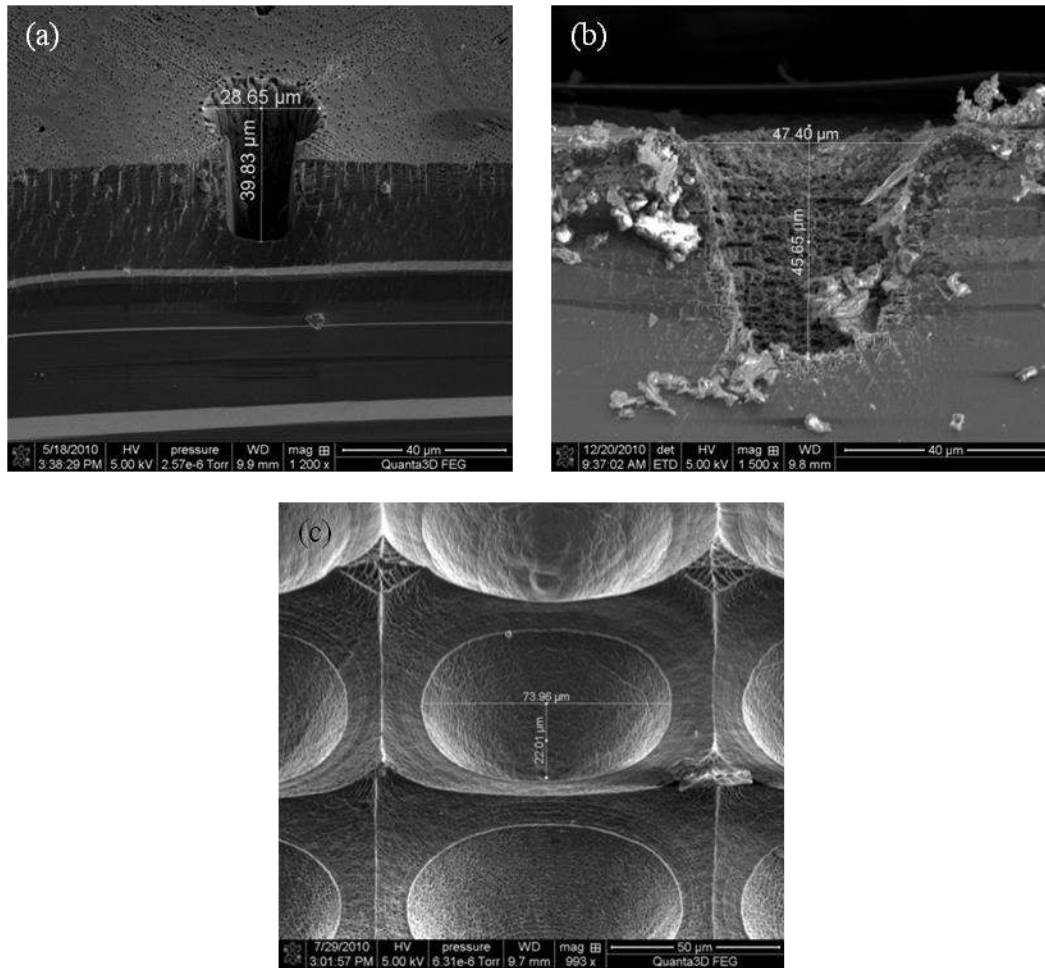
Figure 4.9. SEM images for PEC etched samples at 5V with 632.8 nm at light intensities (a) 92.22 mW/cm^2, (b) 230.55 mW/cm^2, and (c) 461.11 mW/cm^2.

patterned Si is kinetically limited at the same light intensity. Patterned Si reaches transition regime at higher light intensities as compared to the blank Si surface. While mass transfer limitations are expected to be higher in smaller features, our results show reaction in micron sized structure not being limited by mass transfer at the same conditions in which reaction millimeter sized pits is limited by mass transfer. This behavior in microstructures can be explained by the angle of light incidence. KOH pit is used as an etch seed for initiating photoelectrochemical etching in patterned structures while blank Si is subjected to photoelectrochemical etching without KOH etching. Consequently, the angle of incidence of

light is greater in the microstructures, resulting in lesser photon absorption than planar blank Si. Thus, the reaction rate in microstructures is still limited by charge transfer at the same incident light intensity at which the dissolution reaction in millimeter sized pits is limited by mass transfer.

The aspect ratio of the microstructures created by photoelectrochemical etching of patterned n-type Si (10-20 Ω-cm) is obtained as a function of incident light intensity. Figure 4.10
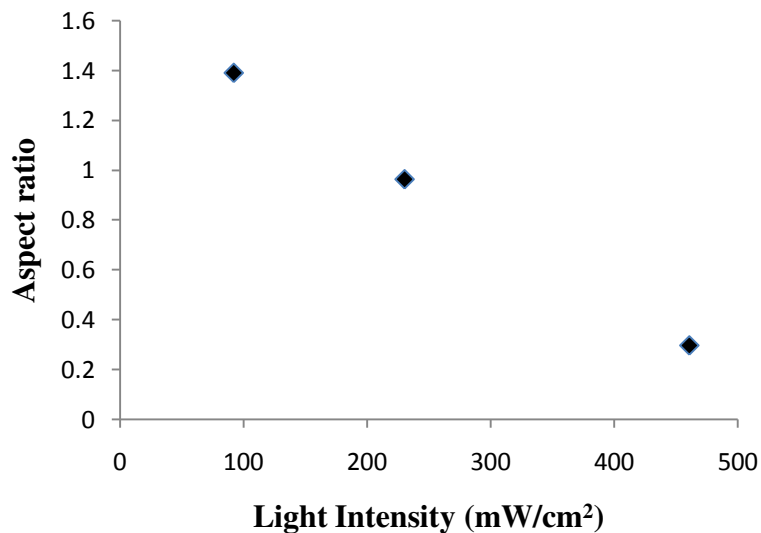
Figure 4.10. Aspect ratio variation in patterned Si as a function of light intensity at an applied bias of 5 V versus Pt.

demonstrates the aspect ratio of the microstructures as a function of the incident light intensity. All the experiments are performed with 6 µm opening diameter and 5 V applied bias. Aspect ratio used in Figure 4.10 suggests only microstructure depth and does not consider total vertical depression created as a result of undercut. As the light intensity increases, lateral expansion becomes more pronounced. Also, undercut increases with the light intensity and has a negative effect on aspect ratio. At light intensities equal to or lower than 92.22 mW/cm^2, photons absorbed from the collimated light contribute to a faster vertical etch rate as compared to the radial etch rate. Whereas at higher light intensities, either Si dissolution mechanism alters to

form an intermediate oxide layer which is subsequently chemically etched by HF giving an isotropic etch or there is excessive undercut leading to a decrease in apparent aspect ratio.

4.1.4 Effect of Surfactants
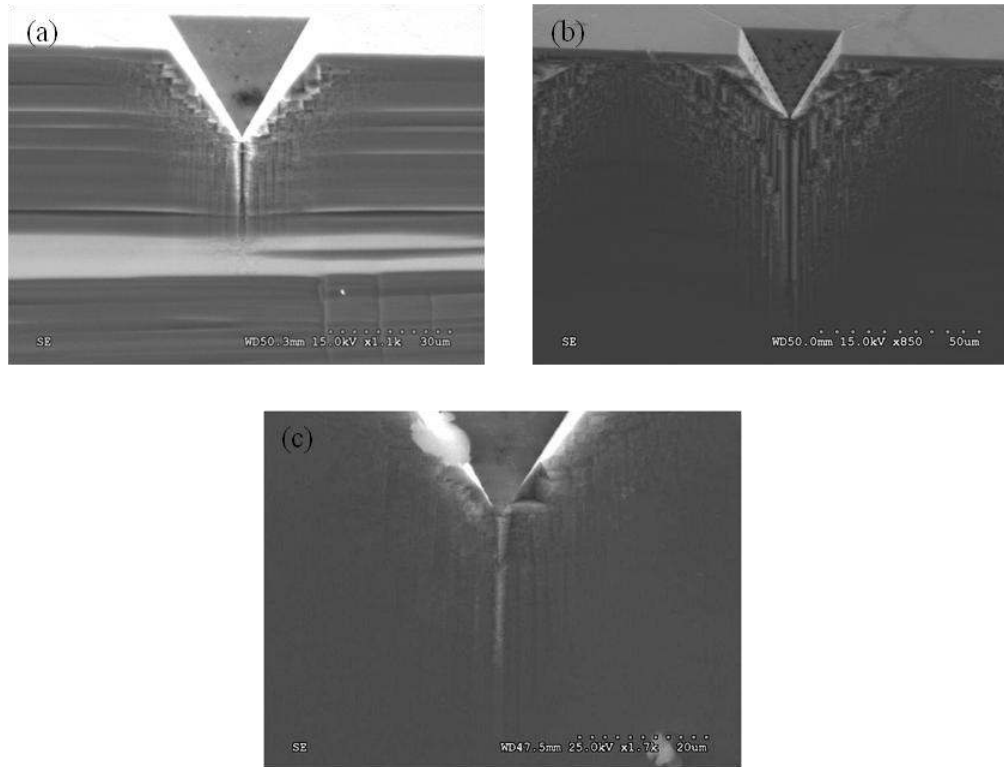
Figure 4.11. SEM images showing the effect of different surfactants in the aq. Electrolyte containing 4.63M HF, 57.77% (vol) IPA, and (a) 74400 ppm Sulfobetaine-12, (b) 13300 ppm DowFax-3B2, and (c) 1480 ppm Triton X-100.

Electrolyte-semiconductor contact can be improved by releasing H_2 gas bubbles formed on Si surface during electrochemical etching. Surfactants improve the electrolyte-semiconductor contact by reducing interfacial surface tension. Effect of different surfactants on etch rate and anisotropy is observed from Figure 4.11. Anionic (DowFax-3B2), Neutral (Triton X-100) and Zwitterionic (Sulfobetaine-12) surfactants are added below their critical micellar concentration in the electrolyte containing 4.63M HF, 57.77 volume % IPA, and water. Experiments were performed on p-type Si (100) with resistivity 10-20 ohm-cm and etched with KOH prior to

45

electrochemical etching. To explore the chemistry of etchants with Si, both n-type and p-type could be used since they only differ in their electronic properties but their chemistry remains similar (Gerischer and Lubke 1987; Lehmann 1993). An attempt was made to adsorb negatively charged surfactant molecules (anionic and zwitterionic) on anodized Si surface to passivate sidewalls. Figure 4.11a and 4.11b confirm neither zwitterions nor anions served in blocking the sidewalls. Instead, these surfactants performed their role as a surfactant by freeing the Si surface from gas bubbles; thereby etch rate is maintained in all crystallographic orientations. Similar action was observed with a neutral surfactant. Although surfactants played no role in the sidewall passivation, their contribution towards improving electrochemical etch rate served as reason for their incorporation in the electrolyte. The etch rate achieved with these surfactants were around 0.5 µm/min. From a qualitative point of view it is observed from Figure 4.11 a, b and c sidewall etching is more vigorous with ionic surfactants as compared to neutral surfactant.

4.1.5 Electrolyte Selection

Dissolution rate observed in each system depends partly on electrolyte composition. Blank n-type Si (100) wafers are used for investigating H_2O and isopropyl alcohol (IPA) effect on the etch rate. In each experimental run, the electrolyte contains 5.1 M HF and 1480 ppm Triton X-100, the average light intensity incident at the silicon-electrolyte interface is 46.11 mW/cm^2 and an anodic potential versus Pt reference is 5 V. Figure 4.12 proves combination of water and IPA in electrolyte enhances etch rate. IPA minimizes solution surface tension thereby causing increased wettability and higher H_2 detachment rates from Si surface (Campbell, Cooper et al. 1995). High wettability has a positive effect on dispersive nature of HF and fluoride (F^-) species in the electrolyte thereby improving mass transfer. As a consequence, limiting current increases at same HF concentration (Lin, Lai et al. 2008). This is observed from Figure 4.13 and 4.8b.
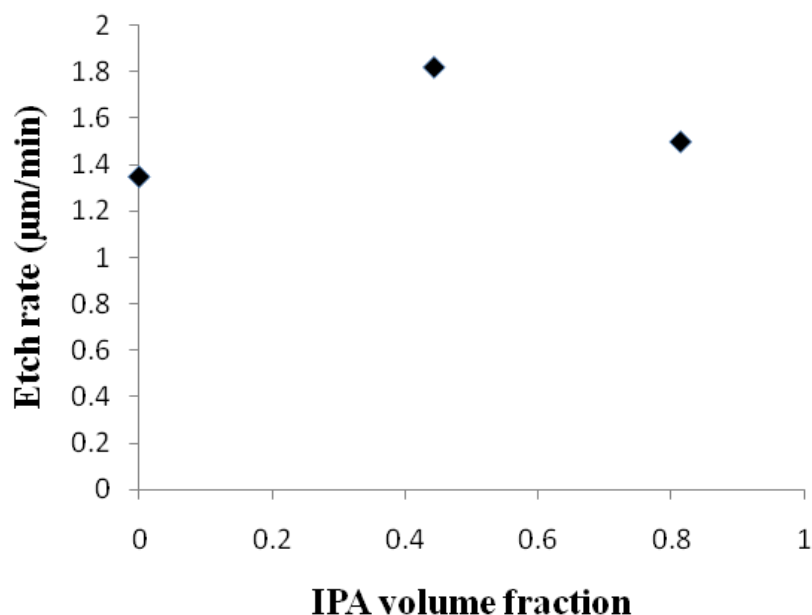
Figure 4.12. Etch rate as function of IPA volume fraction in electrolyte.

Figure 4.13b and 4.13c reveal tangled wire-like microporous structure. Similar structure is obtained when dissolution occurs with charge transfer limiting overall reaction rate (Figure 4.8c). Figure 4.13a shows cup shaped morphology resembling surface morphology attained in transition regime (charge transfer rate = mass transfer rate, Figure 4.8d). IPA's (3.5 µs/cm) larger electrical conductivity than distilled water (0.04 µs/cm) assists in improving the etch rate. Merlos et al also stated IPA's role in reducing undercut by 40-72% (Merlos, Acero et al. 1993). On the other hand, dielectric constant of water (78.39) is higher than IPA (19.9), resulting in higher degree of HF solvation in water. As a result, concentration of F^- ions is higher in the electrolyte containing water. Presence of F^- ions in the electrolyte contribute in improving the Si dissolution rate (Lin, Lai et al. 2008). Thus, a mixture of water and IPA in the supporting electrolyte increases the overall etch rate of the system.
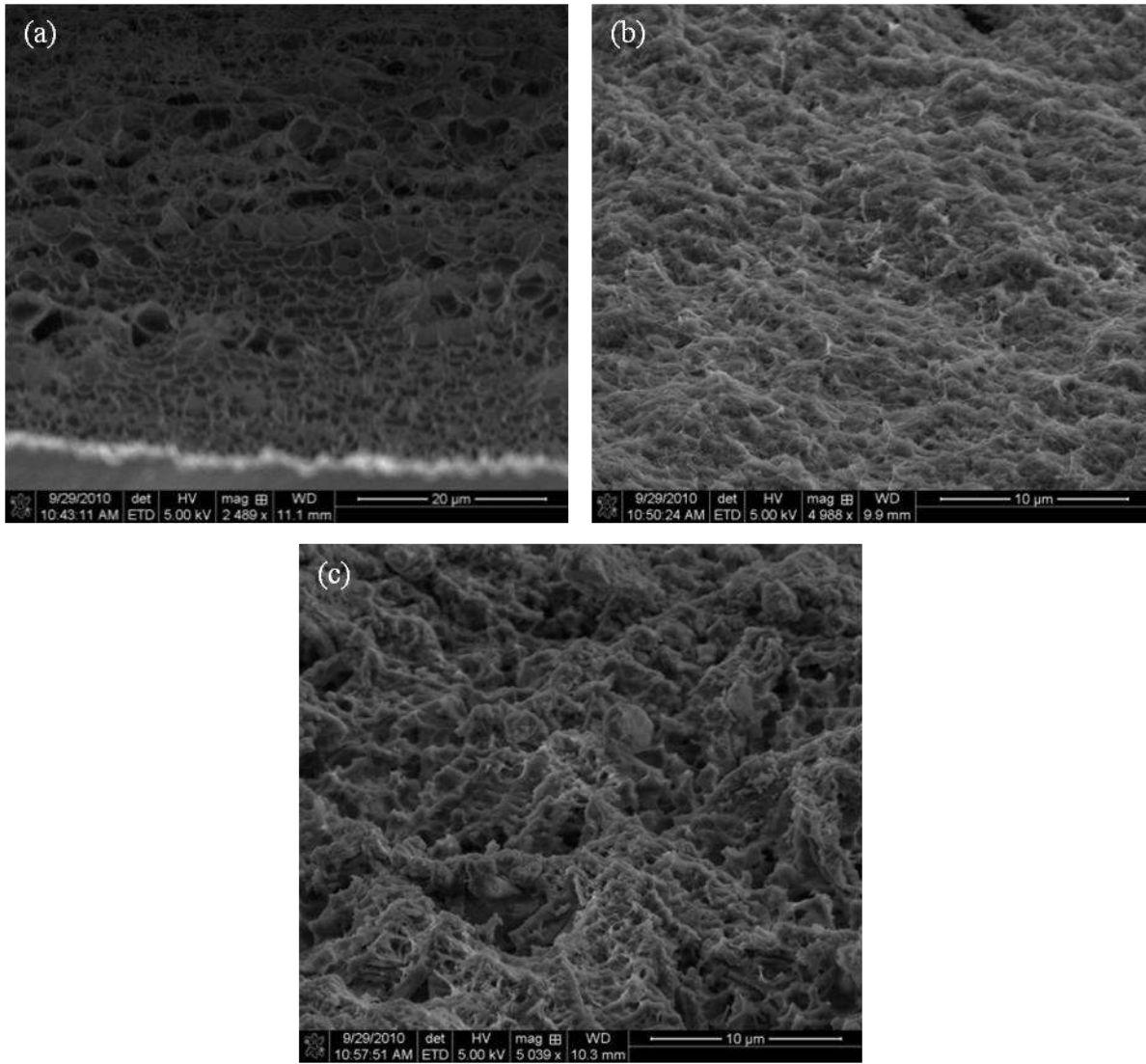
Figure 4.13. Morphology of etch pit with the electrolyte composition as CHF = 5.10M, CTriton X-100 = 1480 ppm, and (a) 92.56% (v/v) water, (b) 11.06% (v/v) water, 81.5% (v/v) IPA, and (c) 44.41% (v/v) water, 48.15% (v/v) IPA.

4.2 Effect of Applied Bias

The effect of applied bias on sidewall porosity of the microstructures is studied. When photons from the incident light are absorbed by Si electron-hole pairs are generated. These photo-generated holes in Si are brought to silicon-electrolyte interface by applied anodic bias. Since we use frontside illumination the electron-hole pairs are generated in the depletion region or in both,

the depletion region and bulk Si. The recombination rate of electron-hole pairs depend on their position relative to the depletion region width. Currents arising during photoelectrochemical etching are categorized based on the position of photon absorption relative to the depletion region in Si.

The depletion region is a strong function of Si resistivity and the applied bias. The relationship between the depletion region width (W_{DR}) and the applied bias (V_{app}) is given by,

$$W_{DR} = \sqrt{\frac{2.\varepsilon_0.\varepsilon_{Si}.V_{eff}}{q.N_D}} \quad (4.1)$$

$$\text{where,} \quad V_{eff} = V_{bi} - V_{app} \quad (4.2)$$

Built-in voltage for Si-HF junctions (V_{bi}) ~ 0.5 (Wehrspohn, Schweizer et al. 2007), Permittivity of free space (ε_0) – 8.85×10^{-14} F·cm^{-1}, Relative permittivity of Si (ε_{Si}) – 11.7, Elementary charge (q) – 1.6×10^{-19} C, Donor concentration (N_D) – 3.604×10^{14} cm^{-3}, Boltzmann's constant (k) – 8.61×10^{-5} eV/K, Intrinsic carrier concentration at 300 K (n_i) – 8.6×10^9 cm^{-3}, and
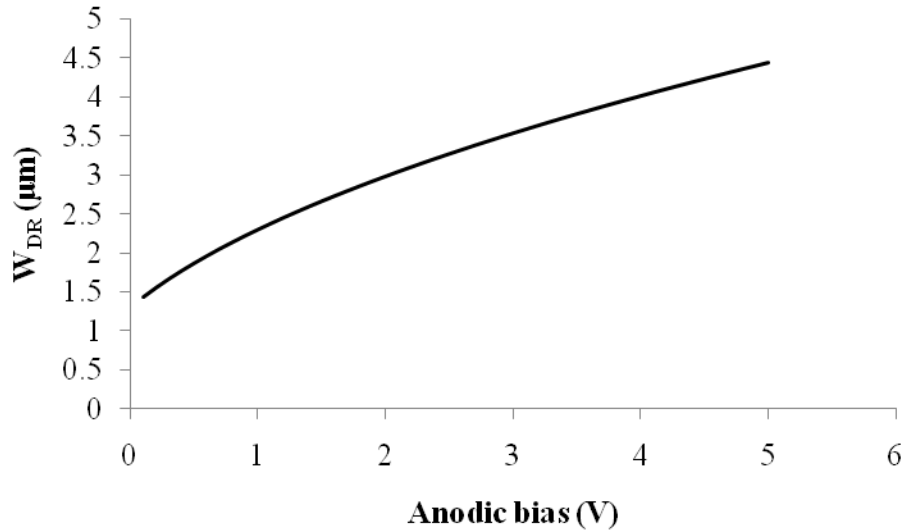
Figure 4.14. Depletion Region Width as function of applied anodic bias for a planar surface n-type Si (100).

Temperature (T) – 300 K. Figure 4.14 shows a plot of the depletion region width as a function of the applied bias for planar n-type Si (10-20 Ω-cm). From Figure 4.14, it is observed as the reverse bias on n-type Si is increased, the depletion region width increases. The calculated values for the planar surface depletion region width shown in table 4.1:

Table 4.1 Depletion region widths at different anodic bias

Applied bias (V)	$W_{DR}(\mu m)$
5	4.47
0.5	1.88
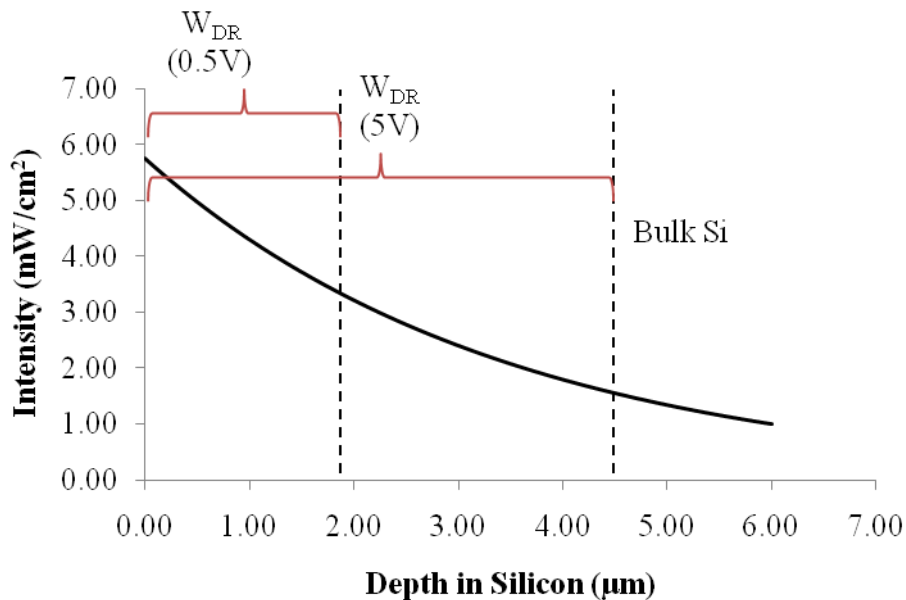
Figure 4.15. Light intensity as a function of depth in Si.

The ability to tailor the depletion region width in Si with given resistivity has made it possible to absorb photons even beyond the depletion region width during frontside illumination. Figure 4.15 shows the schematic for photon absorption as a function of depth in Si. The incident light

has a wavelength of 632.8 nm. Photon absorption in a material is governed by Beer Lambert's law. Beer-Lambert's law shows photon flux (light intensity) as a function of depth (Equation 4.3);

$$I = I_0 . e^{-\alpha.x} \quad (4.3)$$

Where, I' is the light intensity at any depth 'x', 'I_0' is the incident intensity of light, and 'α' is the photon absorption coefficient. Photon absorption coefficient varies with the material and the incident light wavelength. For monochromatic light, the photon absorption coefficient remains constant ($\alpha_{632.8\ nm} = 2.9 \times 10^3$). Consequently, the intensity of light exponentially decays with increasing depth in Si. Area under the intensity versus depth curve gives the number of photons absorbed within the depth considered. The dotted vertical lines in Figure 4.15 indicate the
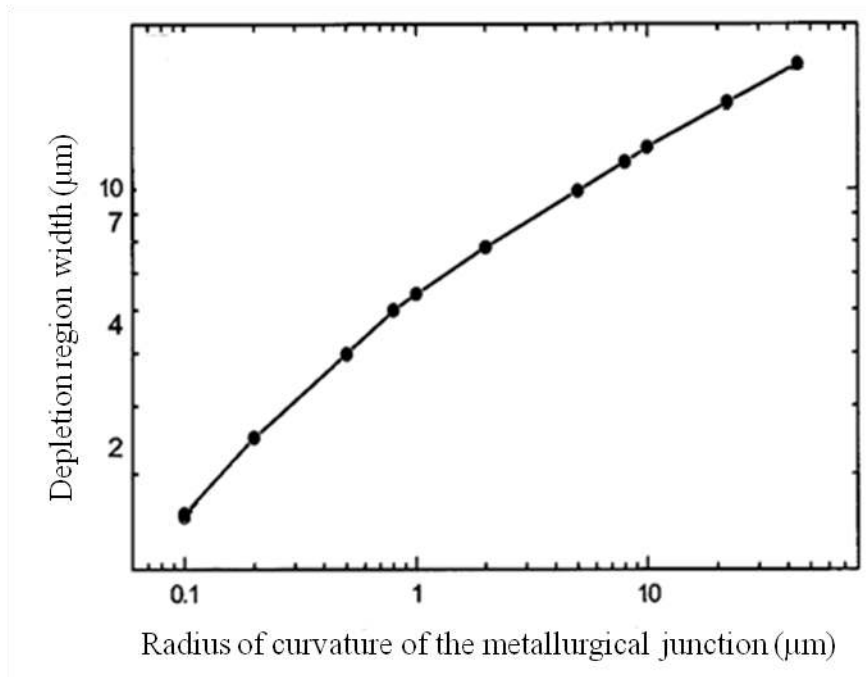
Figure 4.16.Effect of radius of curvature on depletion region width, (Jin, Xuemei et al. 2002)

position of the depletion region and bulk Si interface. The width of the depletion region varies

51

with the applied potential. When the width of the depletion region is large majority of the photons are absorbed within the depletion region, while for a smaller depletion region width most of the photons are absorbed beyond the depletion region and into bulk Si. This is indicated by the schematic in Figure 4.15.

The width of the depletion region and the electric field across the depletion region is affected by the surface geometry. Poisson's equation for an interface is given by,

$$\frac{1}{r^2}\frac{d}{dr}[r^2.\xi(r)] = \frac{\rho(r)}{\varepsilon} \quad (4.4)$$

Where ε is the dielectric constant, r is the radius of curvature, $\xi(r)$ is the electric field, and $\rho(r)$ is the charge density in the depletion region. On integrating the Poisson's equation we get,

$$\xi(x + r_0) = \frac{q.N_D}{3.\varepsilon}[-(x + r_0) + \frac{(r_0+x_d)^3}{(x+r_0)^2}] \quad (4.5)$$

Where, N_D is the ionized dopant density, q is the electronic charge, r_0 is the radius of curvature at the interface, x_D is the depletion region width, r is given as x+r_0 (Zhang 1991). As the radius of

Bulk Si
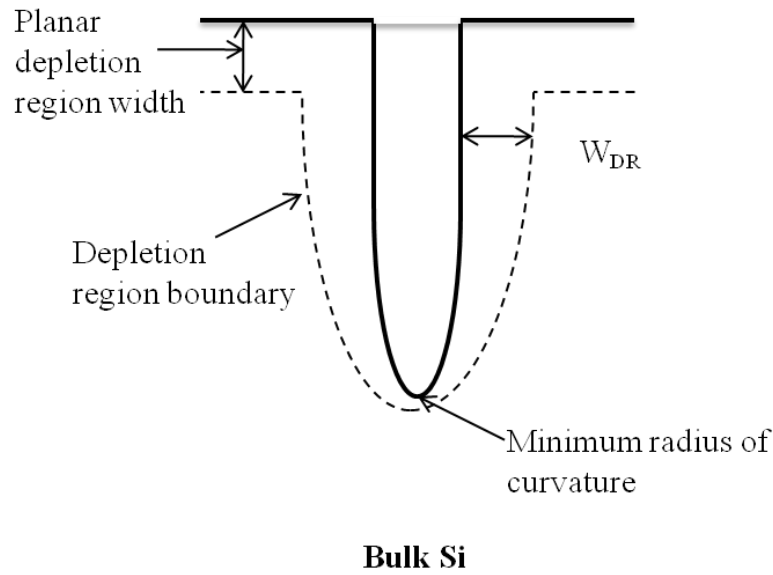
Figure 4.17. Schematic of depletion region width as function of pore geometry.

curvature of the microstructure becomes smaller than the depletion region width of a planar surface, the electric field becomes stronger. This results in high current flow through the region with large electric field. The bottom of a KOH pit or a u-shaped pore has a very small radius of curvature. Thus, the electric field at the bottom of a tapered microstructure is a maximum. A large electric field gives rise to high current flow at the pore tip leading to a higher vertical etch rate.

The depletion region width is a function of the surface geometry. As shown in Figure 4.16, the depletion region width reduces with decreasing radius of curvature of a metallurgical junction (Jin, Xuemei et al. 2002). The planar surface has an infinite value for the radius of curvature. The planar surface depletion region width is the maximum value of the depletion region of Si substrate with a given resistivity at a fixed applied bias. Mellaurgical junction can be approximated to a electrolyte-semiconductor junction. In deep microstructures, the radius of curvature of the microstructure surface varies with every point on the surface. The microstructure tip has the smallest radius of curvature and this gradually increases at the pore walls. Consequently, the depletion region width at the bottom of the microstructures is smaller than at the sidewalls as shown in Figure 4.17.

The investigation on the effect of potential on sidewall porosity of the microstructures is performed at constant average light intensity 11.5 mW/cm^2. Collimated light with 632.8 nm wavelength is used as the photon source. At an applied bias of 5 V highly porous microstructure sidewalls are obtained as shown in Figure 4.18a. As the applied potential is lowered to 0.5 V sidewall porosity reduces (Figure 4.18b). Furthermore, morphology of the microstructures change with the applied bias; at a higher applied bias (5 V versus Pt) microstructure walls are covered with a microporous tangled wire-like layer with macropores at the bottom (Figure 4.18a)

and at lower bias (~ 0.5 -1 V versus Pt) cup shaped smooth structures are formed on the microstructure walls with no microporous layer covering them at a pitch of 50-100 µm (Figure 4.18b). Therefore, lower potentials seem promising to obtain isolated microstructures.

Arita classified the morphology (crystalline or amorphous) of the photoelectrochemically etched blank Si based on the current density. The current density depends on the number of electrons (n) injected into the conduction band of Si during electrochemical etching. 'n' is between 2 and 4 for Si anodization reactions. The electrochemically etched Si structure is amorphous when n is equal to 2 and the Si structure is crystalline for n between 2 and 4. The structure of the electrochemically etched Si (crystalline or amorphous) can be attributed to the relative position of the generation of minority charge carriers with respect to the depletion region. During anodization, n-type Si is under depletion. Current flowing through circuit is composed of drift, diffusion and tunneling currents.

$$J_{Total} = J_{Drift} + J_{Diffusion} + J_{Tunnel} \quad (4.6)$$

Tunneling currents dominate in highly doped Si ($> 10^{18}$/cm^3). Since we are working with 10-20 Ω-cm resistivity (medium doped), tunneling currents are insignificant. Dominance of drift or diffusion current, is based on relative photon absorption position in Si to depletion region width. Drift currents dominate when minority charge carriers are generated within the depletion region (n=2), while the diffusion currents (2<n<4) control Si dissolution reaction, when the charge carriers are generated outside the depletion region (Arita 1978). Further, due to the built in field, almost all the minority charge carriers generated within the depletion region width do not recombine contributing to current (Bazkir 2009). The lifetime of excess carriers is inversely proportional to the recombination rate and ranges from 1 ns to 1 ms in silicon (Delalamo and

54

Swanson 1987) and hence, the excess carriers generated in bulk Si recombine at a certain finite recombination rate.

Microstructures formed in patterned n-type Si (10-20 Ω-cm) show difference in the sidewall porosity based on the relative position of photon absorption with respect to the depletion region.
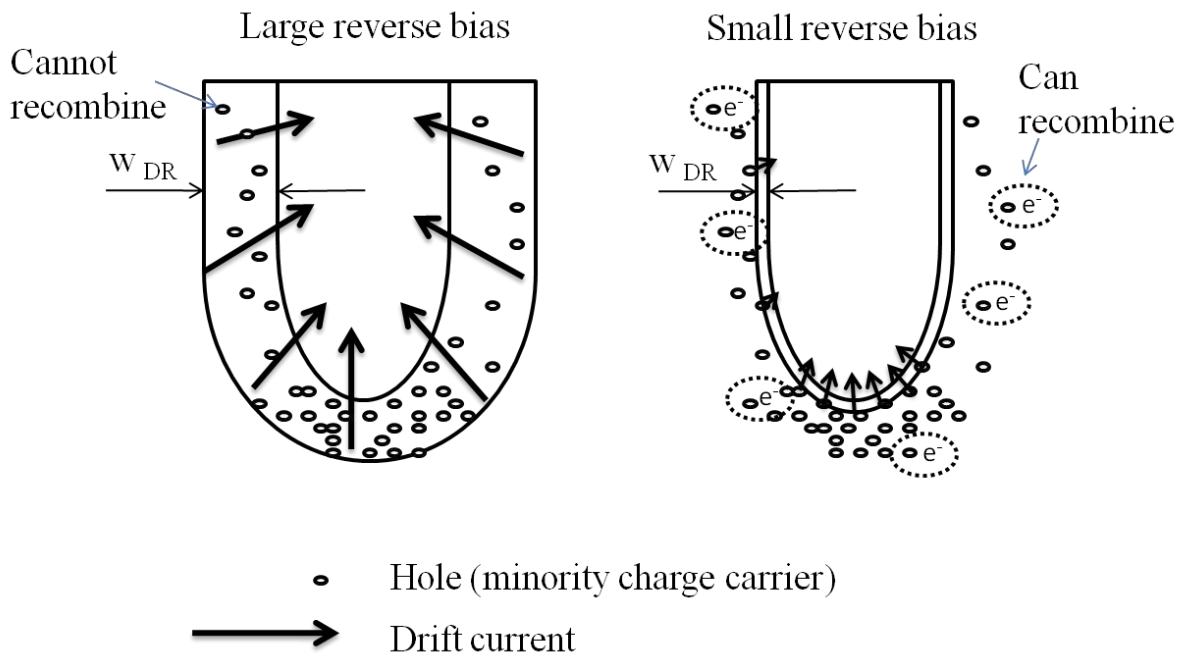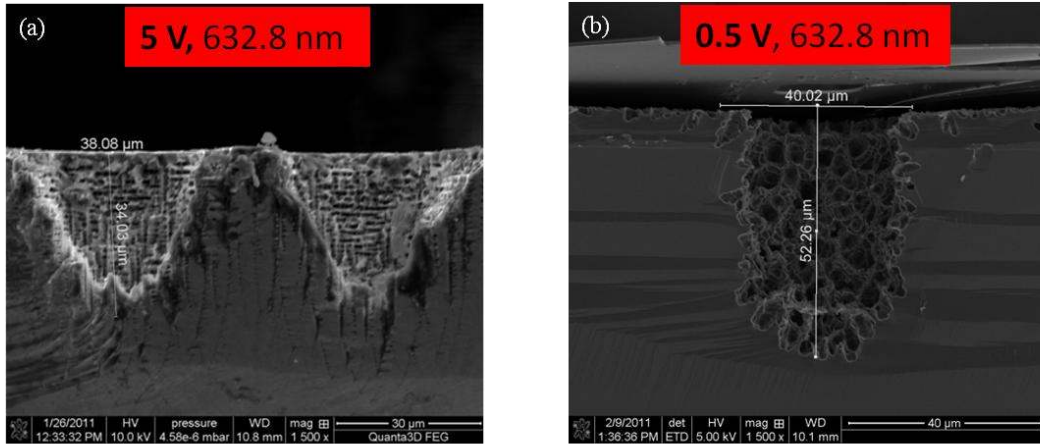
Figure 4.18.Cross-sectional SEM image of TSVs obtained with HeNe laser (632.8 nm) at an applied bias of (a) 5V, (b) 0.5V versus Pt at an average incident light intensity of 11.5 mW/cm^2 (top), schematic showing effect of applied bias (bottom).

Depletion region width increases with increasing reverse bias on n-type Si as per Equation 4.1. For an applied bias of 5 V and 0.5 V, the depletion width is calculated as 4.47 µm and 1.88 µm, respectively. Absorption depth of photons with 632.8 nm wavelength is approximately 3.4 µm (VirginiaSemiconductor). Consequently, at an applied bias of 5 V most of the photons are absorbed within 4.4 µm (depletion region width), while at 0.5 V, majority of the charge carriers are created beyond 1.6 µm. At high reverse bias (5 V) most of the charge carriers are generated in the depletion region. The holes in the depletion region cannot recombine and hence, the electric field drives almost all the holes to the silicon-electrolyte interface. Due to this all the charge carriers generated in the depletion region participate in the Si dissolution reaction giving rise to significant drift currents. Drift currents cause new lattice defects nucleation (Outemzabet, Gabouze et al. 2005) which explains sub-micron sized pores emerging from the sidewalls. On the other hand, when the applied anodic bias is low, the depletion region is extremely thin. Hence, most charge carriers are absorbed beyond the depletion region. These charge carriers generated in the bulk can recombine at a finite recombination rate. The electron-hole pair recombination leads to annihilation of excess carriers. The recombination process reduces the number of holes reaching the depletion region from bulk. The density of holes at the sidewalls is minimized to a great extent due to (i) control over the photon absorption by increased angle of incidence of light at the sidewalls and, (ii) the recombination process occurring in the bulk (when photon absorption occurs beyond the depletion region). At the bottom of the KOH pit due to zero angle of incidence of light larger number of holes are created. A fraction of the holes created beyond the depletion region recombine. The difference in the number of holes generated varies drastically from the sidewalls to the bottom of the microstructure. Thus, majority of holes are present at the bottom of the KOH pit. These holes diffuse to the depletion region and then

brought to the silicon-electrolyte interface by the electric field. (Figure 4.18 bottom). We believe the electron-hole recombination in addition to the lower photon absorption at the sidewalls due to the increased angle of incidence of light at the walls of the KOH pit creates anisotropic isolated structures in n-type Si with frontside illumination.

The dependence of the depletion region width on surface geometry helps in analyzing the effect
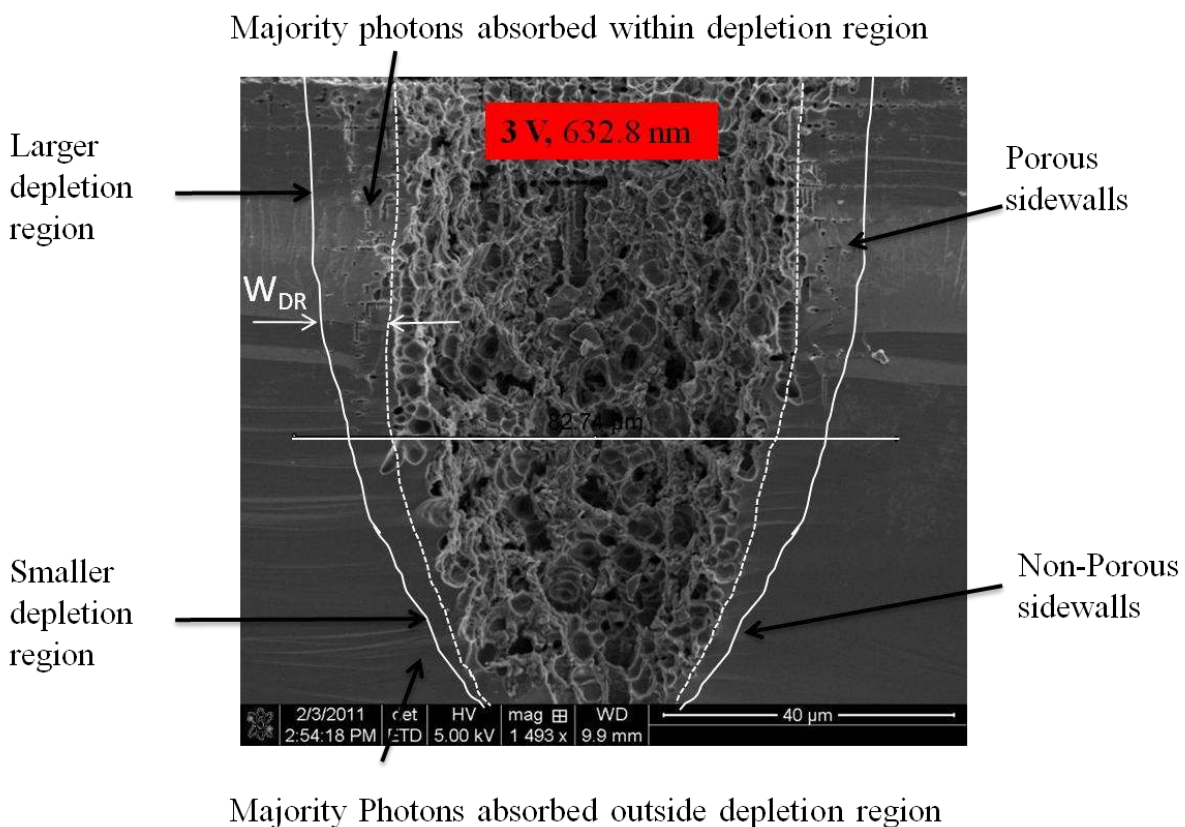
Figure 4.19. SEM image of a single microstructure demonstrating porous and non-porous sidewalls.

of depletion region width on sidewall porosity from the SEM image of a single microstructure. Collimated light (λ = 632.8 nm) with an average light intensity of 115.27 mW/cm^2 is used to illuminate Si. Photoelectrochemical etching is performed at an anodic bias of 3 V. At these conditions, the cross-sectional SEM of a single microstructure is seen from Figure 4.19. The

upper portion of the microstructure shows porous sidewalls, whereas the lower portion shows non-porous sidewalls. The observation of different structures in a single microstructure can be attributed to the depletion region width which varies as a function of microstructure geometry. As the radius of curvature of a surface increases, the depletion region width correspondingly reduces. Consequently, the depletion region width is lesser at the bottom of the microstructure than the top. Thus, majority photons are absorbed within the depletion width at surfaces with smaller radii of curvature (top portion of the microstructure), while majority photons are absorbed beyond the depletion region width at surfaces with larger radii of curvature (bottom curved portion of the microstructure). The electron-hole pairs created in the depletion region do not recombine and consequently lead to excessive nucleation at the sidewalls. While the hole density is reduced when most of the photons are absorbed in the bulk since the recombination rate is much higher in the bulk. These holes created in the bulk with the ability to recombine reduce the percentage of holes reaching the silicon-electrolyte interface.

A low anodic bias decreases the depletion region width thereby generating a larger percentage of excess carriers in the bulk than within the depletion region. Recombination in the bulk helps reduces the drift current thereby reducing nucleation at the sidewalls of the microstructure. Thus, non-porous, isolated microstructures can be created by performing photoelectrochemical etching at a low anodic bias.

4.3 Effect of Wavelength

The effect of wavelength of the incident light on the morphology of photoelectrochemically etched Si is investigated. On illumination, absorption coefficient which is a function of photon energy and absorbing material, governs depth at which photons are absorbed from silicon-electrolyte interface.
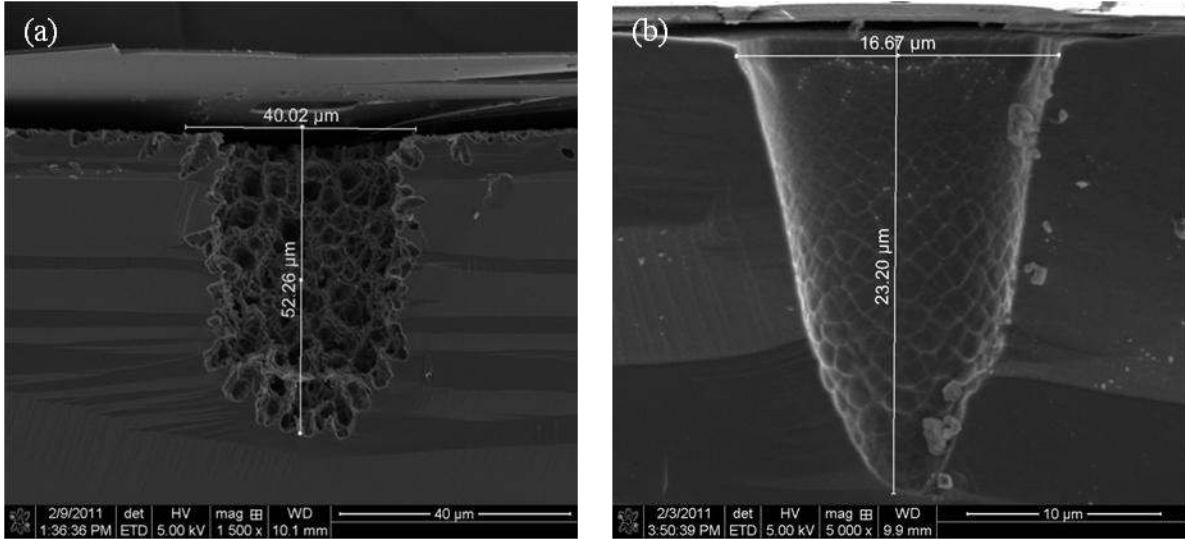
Figure 4.20. Cross-sectional SEM images of TSVs showing morphology variation with photon energy; (a) λ = 632.8 nm, (b) λ = 365nm.
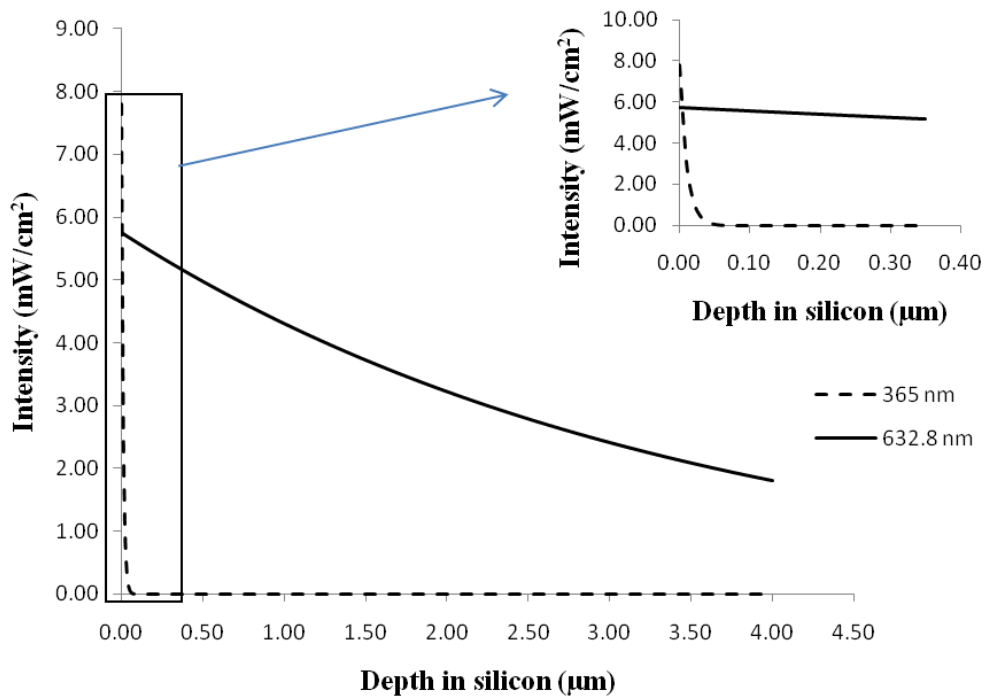
Figure 4.21. Light intensity decay as a function of depth in silicon and the wavelength of light.

Experiments are performed with 632.8 nm HeNe laser and 365 nm collimated UV Light Emitting Diode. Average light intensities of 11.5 mW/cm^2 and 7.8 mW/cm^2 are obtained from

632.nm HeNe laser and the 365 nm UV LED, respectively. Since the average light intensities are almost equal, wavelength is the main parameter varied in both the experiments. Figure 4.20a shows very rough morphology and pronounced cup shaped structures (< 10 µm deep) all along the periphery of the microstructure when irradiated with 632.8 nm light, while Figure 4.20b shows extremely shallow cup shaped structures at the lower half of the microstructures created with 365 nm UV light. There is no evidence of a microporous sidewall at the low applied voltage of 0.5V versus Pt, the incident light intensity and wavelength. The difference in the morphology observed with different wavelengths could be attributed to difference in photon absorption coefficient in Si with the wavelength of the light.

The hole generation rate (g(x)) in a semiconductor is given by the following equation

$$g(x) = I_0. \alpha. e^{-\alpha.x} \quad (4.7)$$

Where, I_0 is the intensity of incident light, I is the intensity at depth x, and α is the absorption coefficient. Equation 4.3 and 4.7 suggest the intensity of light and the hole generation rate decrease exponentially with increasing depth in the absorbing material. Figure 4.21 shows the light intensity decay for 365 nm and 632.8 nm light. The light intensity (photon flux) decay is a strong function of the absorption coefficient of light in Si. Light with smaller wavelengths have higher absorption coefficient. As a consequence, light with 365 nm decays faster with depth than light with 632.8 nm. Photons having a wavelength of 365 nm are absorbed near the silicon-electrolyte interface, whereas the 632.8 nm wavelength photons generate holes from the silicon-electrolyte interface to larger depths in Si. The photon absorption depth (inverse of photon absorption coefficient) corresponding to 632.8 nm is 3.44 µm and 365 nm is 10.5nm (Green and Keevers 1995). The difference in the photon absorption depth is around 2 orders of magnitude.

This difference is evident in the surface roughness of the samples illuminated by light sources with 365 nm and 632.8 nm (Figure 4.20).
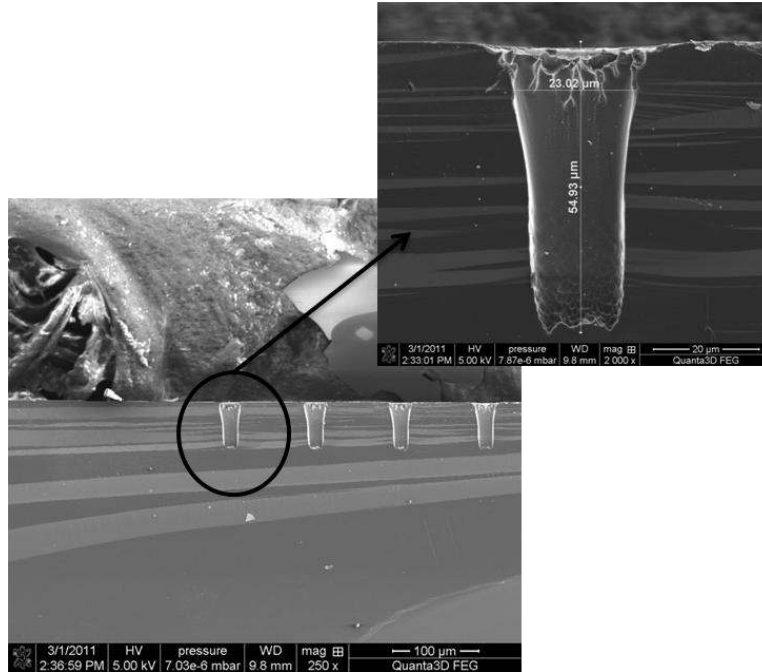
Figure 4.22. SEM image showing anisotropic, isolated microstructures at the corner row of a pattern.

The ideal technique to measure the degree of isolation (non-porous walls) of a microstructure is obtaining the cross-section showing the corner row of a pattern. At the corner row one side of the microstructures is bound by the adjacent microstructure while the other side remains unbound. Figure 4.22 shows the cross-section revealing the corner of a pattern; the sidewalls are non-porous and appear to be the same as the walls bound by other microstructures. Thus, it is feasible to obtain a single isolated microstructure using wet photoelectrochemical etching.

The data points used in Figure 4.23 and 4.24 are as follows:

'1' - Photoelectrochemical etching with Frontside illumination (FSI) on n-type-Si (10-20 Ω-cm)

'2' - KOH Etching

61

'3' - Photoelectrochemical etching with Backside illumination (BSI) on n-type Si (80 Ω-cm), (Lehmann and Foll 1990)

'4' - Photoelectrochemical etching with Backside illumination on n-type Si (20 Ω-cm), (Lehmann and Foll 1990)

'5' - Photoelectrochemical etching with Backside illumination on n-type Si (40 Ω-cm), (Lehmann and Ronnebeck 1999)

'6' - Photoelectrochemical etching with Backside illumination on n-type Si (2.4-4 Ω-cm), (Barillaro, Nannini et al. 2002)
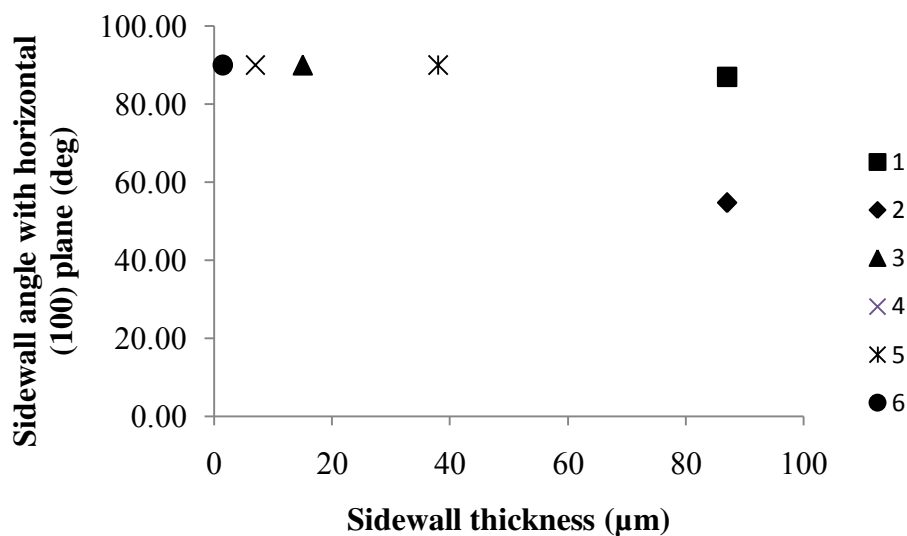
Figure 4.23. Plot comparing frontside illumination with backside illumination and KOH etching to demonstrate sidewall angle as a function of sidewall thickness while creating microstructures with non-porous sidewalls

From Figure 4.23 we observe frontside illumination creates non-porous microstructures with sidewall thickness of 87 µm (wall thickness between adjacent microstructures), while the maximum non-porous sidewall thickness published with backside illumination is approximately 38 µm (Lehmann and Ronnebeck 1999). The non-porous sidewall thickness in microstructures

depends mostly on the depletion region width while using backside illumination for photoelectrochemical etching. The depletion region width restricts the non-porous sidewall
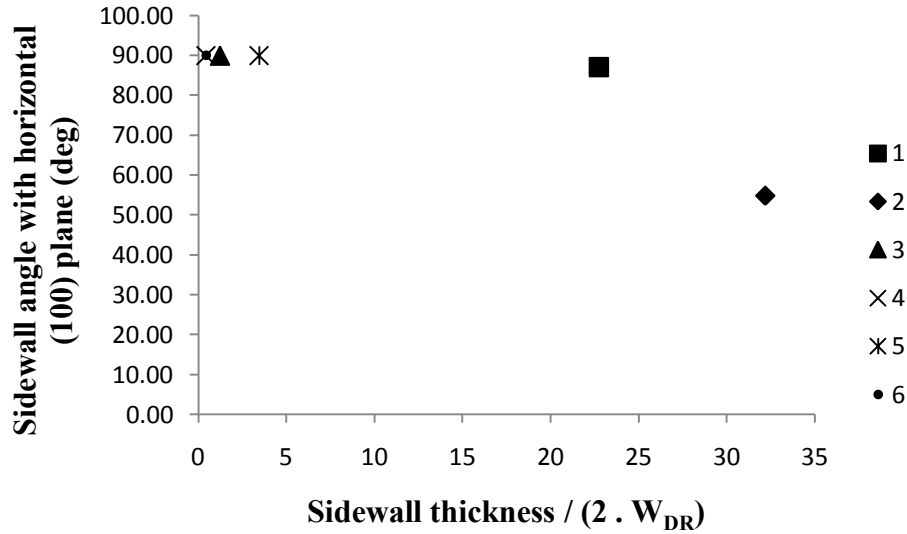
Figure 4.24. Sidewall angle as a function of normalized non-porous sidewall thickness for frontside illumination, backside illumination and KOH etching.

thickness while forming microstructures at isolated locations by backside illumination for a given Si resistivity. The limitation of backside illumination in creating non-porous sidewalls at wall thickness much greater than twice the depletion region width can be observed from Figure 4.24 and 4.25. Figure 4.24 illustrates the microstructure sidewall angle against horizontal (100) plane as a function of the sidewall thickness normalized to twice the depletion region width for non-porous sidewalled microstructures created using frontside illumination, backside illumination and KOH etching. From the plot it is evident that the backside illumination fails to create microstructures or macropores with non-porous sidewalls at larger sidewall thickness (isolated locations). Lehmann and Ronnebeck have shown macropores with non-porous sidewalls up to three times twice the depletion region width with backside illumination (Lehmann and Ronnebeck 1999). Contrary to the result obtained by Lehmann et al, many researchers have observed porous sidewalls at wall thickness greater than twice the depletion

region width (Lehmann and Foll 1990; Barillaro, Nannini et al. 2002; Tao and Esashi 2005; Astrova and Fedulova 2009). From data point 2 it is seen that KOH etching is independent of the wall thickness between the adjacent patterns. However, KOH etching creates sidewalls at 54.74° with (100) plane (horizontal) giving an inverted pyramidal structure. Also, the aspect ratio given as the ratio of height to the diameter of the microstructure remains constant with time. On the other hand, data point 1 proves that photoelectrochemical etching with frontside illumination can create microstructures independent of the wall thickness between the adjacent patterns ((sidewall thickness / 2 × depletion region width) = 22.76) and the angle made by the sidewalls is approximately 87° with the horizontal.
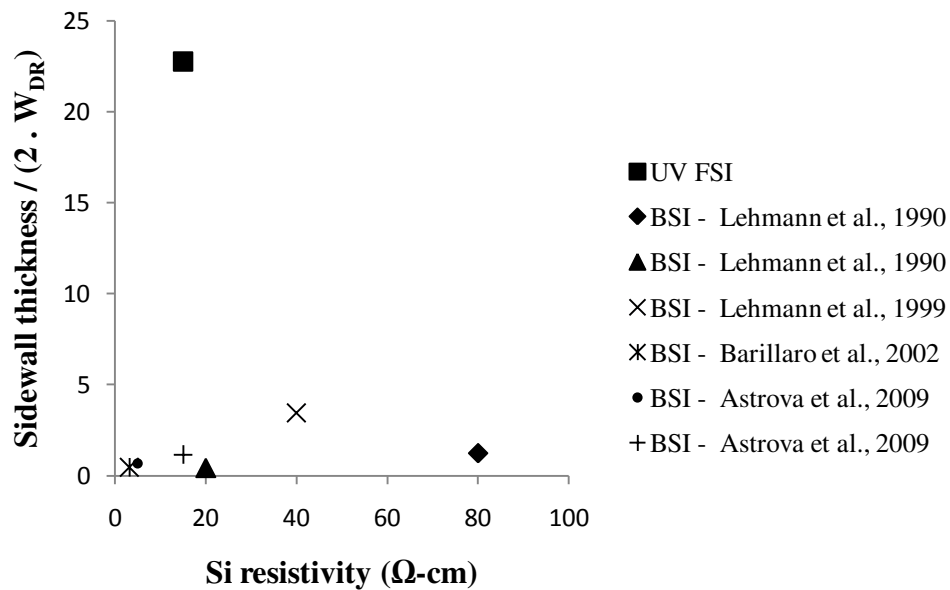
Figure 4.25. Plot of normalized non-porous sidewall thickness at different n-type Si resistivites. Since the sidewall thickness of isolated microstructures using backside illumination is a function of Si resistivity, the sidewall thickness normalized to twice the depletion region width is plotted against Si resistivity in Figure 4.25. This plot indicates for n-type Si 10-20 Ω-cm, a normalized sidewall thickness of 22.76 and 1.165 (Astrova and Fedulova 2009) for frontside illumination

and backside illumination, respectively, suggesting photoelectrochemical etching using frontside illumination using UV light source (365 nm) and low applied reverse bias (0.5 V) has the potential to create isolated microstructures in n-type Si (100) 10-20 Ω-cm.
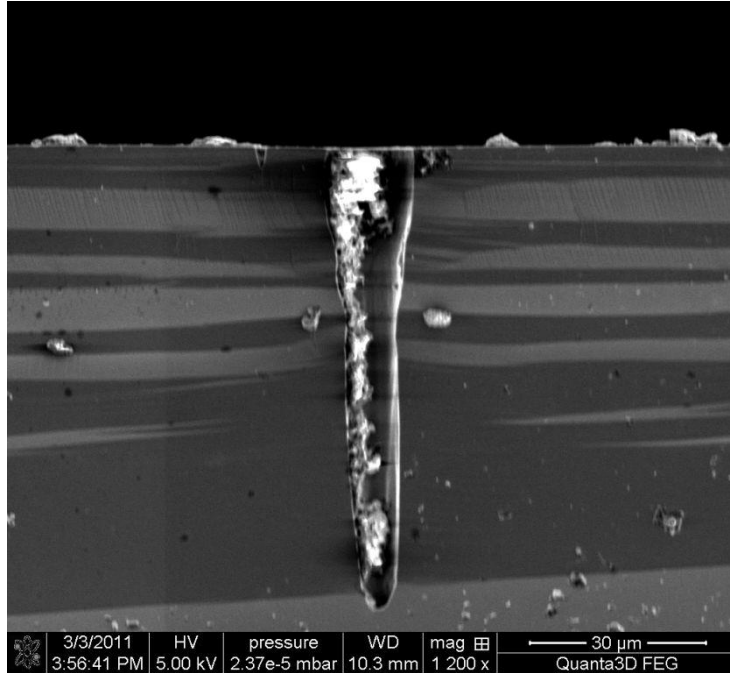
Figure 4.26. Photo-electrochemical etching of n-type Si at 0.5 V versus Pt using 7.8 mA/cm2 average light intensity from 365 nm collimated UV LED for 4 hours.

Prolonged etch for 4 h using UV light source (365 nm) at an average incident light intensity of 7.8 mA/cm^2, a maximum depth of 78 – 96 µm is repeatedly obtained giving an overall etch rate of 0.325 – 0.4 µm/min. Sidewalls making 85-90º with horizontal axis were obtained. Moreover, a minimal radial expansion of 2-3 µm from the initial seed size is observed. Isolated microstructuress are created at a pitch of 100 µm (Figure 4.26). Further, the aspect ratio increases with time, hence, anisotropic, isolated, high aspect ratio microstructures can be fabricated.

5   CONCLUSION

Effect of incident light wavelength, and applied bias have been studied to create high aspect ratio, and anisotropic microstructures at isolated locations in n-type silicon (Si), via wet photoelectrochemical etching using frontside illumination. Lehmann et al observed excessive lateral etching due to near surface charge carrier generation while using frontside illumination. Contrary to the observation by Lehmann et al, high aspect ratio microstructures have been demonstrated in this work using frontside illumination. Moreover, the depletion region no longer serves as the sidewall passivating agent while illuminating at the silicon-electrolyte interface. Microstructures with an aspect ratio of approximately 5:1 have been obtained and the aspect ratio increases with time. Etch rate is a function of the light intensity while working in charge transfer limited regime, necessary condition for anisotropic etching.

Minority carrier generation beyond the depletion region width on application of low reverse bias, reduces sidewall porosity and leads to the formation of microstructures with non-porous sidewalls at isolated locations. The morphology of the microstructures is found to be a strong function of the incident wavelength. The microstructure wall roughness could be attributed to the absorption depth of the incident light; consequently smooth sidewalls are obtained with smaller wavelength illumination. Furthermore, use of UV light with photon energy greater than band gap of silicon nitride helps in eliminating chrome and gold masking layers.

.

REFERENCES

Al Rifai, M. H., H. Christophersen, et al. (2000). "Dependence of macropore formation in n-Si on potential, temperature, and doping." Journal of the Electrochemical Society **147**(2): 627-635.

Albuyaron, A., S. Bastide, et al. (1993). "MORPHOLOGY OF POROUS N-TYPE SILICON OBTAINED BY PHOTOELECTROCHEMICAL ETCHING .2. STUDY OF THE TANGLED SI WIRES IN THE NANOPOROUS LAYER." Journal of Luminescence **57**(1-6): 67-71.

Arita, Y. (1978). "FORMATION AND OXIDATION OF POROUS SILICON BY ANODIC REACTION." Journal of Crystal Growth **45**(1): 383-392.

Astrova, E. V. and G. V. Fedulova (2009). "Formation of deep periodic trenches in photo-electrochemical etching of n-type silicon." Journal of Micromechanics and Microengineering **19**(9).

Badel, X., J. Linnros, et al. (2003). "Electrochemical etching of n-type silicon based on carrier injection from a back side p-n junction." Electrochemical and Solid State Letters **6**(6): C79-C81.

Bao, X. Q., J. W. Jiao, et al. (2007). "Macropore formation without illumination on low doped n-type silicon." Journal of the Electrochemical Society **154**(3): D175-D181.

Bao, X. Q., J. W. Jiao, et al. (2007). "Fast speed pore formation via strong oxidizers." Electrochimica Acta **52**(24): 6728-6733.

Barillaro, G., P. Bruschi, et al. (2005). "Fabrication of regular silicon microstructures by photo-electrochemical etching of silicon." physica status solidi (c) **2**(9): 3198-3202.

Barillaro, G., A. Nannini, et al. (2002). "Electrochemical etching in HF solution for silicon micromachining." Sensors and Actuators a-Physical **102**(1-2): 195-201.

Barycka, I. and I. Zubel (1995). "SILICON ANISOTROPIC ETCHING IN KOH-ISOPROPANOL ETCHANT." Sensors and Actuators a-Physical **48**(3): 229-238.

Bazkir, O. (2009). "QUANTUM EFFICIENCY DETERMINATION OF UNBIASED SILICON PHOTODIODE AND PHOTODIODE BASED TRAP DETECTORS." Reviews on Advanced Materials Science **21**(1): 90-98.

Bhattacharya, E., H. A. Rani, et al. (2005). "Effect of porous silicon formation on stiction in surface micromachined MEMS structures." Physica Status Solidi a-Applications and Materials Science **202**(8): 1482-1486.

Blaw, M. A., T. Zijlstra, et al. (2001). "Balancing the etching and passivation in time-multiplexed deep dry etching of silicon." Journal of Vacuum Science & Technology B **19**(6): 2930-2934.

Campbell, S. A., K. Cooper, et al. (1995). "INHIBITION OF PYRAMID FORMATION IN THE ETCHING OF SI P 100 IN AQUEOUS POTASSIUM HYDROXIDE-ISOPROPANOL." Journal of Micromechanics and Microengineering **5**(3): 209-218.

Delalamo, J. A. and R. M. Swanson (1987). "MODELING OF MINORITY-CARRIER TRANSPORT IN HEAVILY DOPED SILICON EMITTERS." Solid-State Electronics **30**(11): 1127-1136.

Denda, S. (2007). Process Examination of Through Silicon Via Technologies. Polymers and Adhesives in Microelectronics and Photonics, 2007. Polytronic 2007. 6th International Conference on.

Flake, J. C., M. M. Rieger, et al. (1999). "Electrochemical etching of silicon in nonaqueous electrolytes containing hydrogen fluoride or fluoroborate." Journal of the Electrochemical Society **146**(5): 1960-1965.

Foll, H., M. Christophersen, et al. (2002). "Formation and application of porous silicon." Materials Science & Engineering R-Reports **39**(4): 93-141.

Forsman, A. C., E. H. Lundgren, et al. (2007). "Double-pulse format for improved laser drilling - Second pulse enhances both drilling speed and hole quality." Photonics Spectra **41**(9): 72-+.

Franz Laermer, A. S. (2002). Method of anisotropic etching of silicon.

Gad-el-Hak, M. (2005). MEMS: design and fabrication. G.-e.-H. M., Taylor and Francis Group. **second edition**.

Galun, E., R. Tenne, et al. (1993). "ROOM-TEMPERATURE PHOTOLUMINESCENCE OF PHOTOELECTROCHEMICALLY ETCHED N-TYPE SI." Journal of Luminescence **57**(1-6): 125-129.

Gerische.H and W. Mindt (1968). "MECHANISMS OF DECOMPOSITION OF SEMICONDUCTORS BY ELECTROCHEMICAL OXIDATION AND REDUCTION." Electrochimica Acta **13**(6): 1329-&.

Gerischer, H. and M. Lubke (1987). "THE ELECTROCHEMICAL-BEHAVIOR OF N-TYPE SILICON (111)-SURFACES IN FLUORIDE CONTAINING AQUEOUS-ELECTROLYTES." Berichte Der Bunsen-Gesellschaft-Physical Chemistry Chemical Physics **91**(4): 394-398.

Green, M. A. and M. J. Keevers (1995). "OPTICAL-PROPERTIES OF INTRINSIC SILICON AT 300 K." Progress in Photovoltaics **3**(3): 189-192.

Guozheng, W., F. Shencheng, et al. (2010). "Influence of voltage on photo-electrochemical etching of n-type macroporous silicon arrays." Journal of Semiconductors **31**(11): 116002-116001 - 116002-116005.

Guozheng, W., F. Shencheng, et al. (2008). Optimization of macropore silicon morphology etched by photo-electrochemistry. Solid-State and Integrated-Circuit Technology, 2008. ICSICT 2008. 9th International Conference on.

Harraz, F. A., K. Kamada, et al. (2005). "Pore filling of macropores prepared in p-type silicon by copper deposition." Physica Status Solidi a-Applications and Materials Science **202**(8): 1683-1687.

Hu, S. M. and D. R. Kerr (1967). "OBSERVATION OF ETCHING OF N-TYPE SILICON IN AQUEOUS HF SOLUTIONS." Journal of the Electrochemical Society **114**(4): 414-&.

Jansen, H., H. Gardeniers, et al. (1996). "A survey on the reactive ion etching of silicon in microtechnology." Journal of Micromechanics and Microengineering **6**(1): 14-28.

Jin, H., X. Xuemei, et al. (2002). "Equivalent junction method to predict 3-D effect of curved-abrupt p-n junctions." Electron Devices, IEEE Transactions on **49**(7): 1322-1325.

Kim, H. C., D. H. Kim, et al. (2006). "Photo-assisted electrochemical etching of a nano-gap trench with high aspect ratio for MEMS applications." Journal of Micromechanics and Microengineering **16**(5): 906-913.

Kim, J. H., K. P. Kim, et al. (2008). "Macropore Formation in Prepatterned p-type Silicon." ECS Transactions **16**(3): 291-297.

Koker, L. and K. W. Kolasinski (2000). "Photoelectrochemical etching of Si and porous Si in aqueous HF." Physical Chemistry Chemical Physics **2**(2): 277-281.

Koker, L. and K. W. Kolasinski (2001). "Laser-assisted formation of porous Si in diverse fluoride solutions: Reaction kinetics and mechanistic implications." Journal of Physical Chemistry B **105**(18): 3864-3871.

Kolasinski, K. W. (2003). "The mechanism of Si etching in fluoride solutions." Physical Chemistry Chemical Physics **5**(6): 1270-1278.

Kolasinski, K. W. (2009). "Etching of silicon in fluoride solutions." Surface Science **603**(10-12): 1904-1911.

Lehmann, V. (1993). "THE PHYSICS OF MACROPORE FORMATION IN LOW DOPED N-TYPE SILICON." Journal of the Electrochemical Society **140**(10): 2836-2843.

Lehmann, V. and H. Foll (1990). "FORMATION MECHANISM AND PROPERTIES OF ELECTROCHEMICALLY ETCHED TRENCHES IN N-TYPE SILICON." Journal of the Electrochemical Society **137**(2): 653-659.

Lehmann, V. and U. Gosele (1992). "POROUS SILICON - QUANTUM SPONGE STRUCTURES GROWN VIA A SELF-ADJUSTING ETCHING PROCESS." Advanced Materials **4**(2): 114-116.

Lehmann, V. and S. Ronnebeck (1999). "The physics of macropore formation in low-doped p-type silicon." Journal of the Electrochemical Society **146**(8): 2968-2975.

Levyclement, C., A. Lagoubi, et al. (1993). "POROUS N-SILICON PRODUCED BY PHOTOELECTROCHEMICAL ETCHING." Applied Surface Science **65-6**: 408-414.

Levyclement, C., A. Lagoubi, et al. (1994). "MORPHOLOGY OF POROUS N-TYPE SILICON OBTAINED BY PHOTOELECTROCHEMICAL ETCHING .1. CORRELATIONS WITH MATERIAL AND ETCHING PARAMETERS." Journal of the Electrochemical Society **141**(4): 958-967.

Li, X., H. S. Seo, et al. (2009). "A periodic array of silicon pillars fabricated by photoelectrochemical etching." Electrochimica Acta **54**(27): 6978-6982.

Lim, P., J. R. Brock, et al. (1992). "LASER-INDUCED ETCHING OF SILICON IN HYDROFLUORIC-ACID." Applied Physics Letters **60**(4): 486-488.

Lin, J. C., C. M. Lai, et al. (2008). "Effect of ethanol on the photoelectrochemical fabrication of macroporous N-Si(100) in HF solution." Journal of the Electrochemical Society **155**(6): D436-D442.

Lin, J. C., W. C. Tsai, et al. (2007). "The enhancement of photoluminescence of n-type porous silicon by Hall-effect assistance during electrochemical anodization." Electrochemistry Communications **9**(3): 449-453.

Lu, K. H., Z. Xuefeng, et al. (2009). Thermo-mechanical reliability of 3-D ICs containing through silicon vias. Electronic Components and Technology Conference, 2009. ECTC 2009. 59th.

Luft, A., U. Franz, et al. (1996). "A study of thermal and mechanical effects on materials induced by pulsed laser drilling." Applied Physics a-Materials Science & Processing **63**(2): 93-101.

Lust, S. and C. Levy-Clement (2002). "Chemical limitations of macropore formation on medium-doped p-type silicon." Journal of the Electrochemical Society **149**(6): C338-C344.

M.Puech, N. l., N.Arnal,P.Godinat,JM.Gruffat (2002). <u>A Novel Plasma Release Process and a Super High Aspect Ratio Process using ICP Etching for MEMS</u>. 6th SEMIMicrosystems/MEMS Seminar.

Many, A., M. Wolovelsky, et al. (1993). "SURFACE-STATES AT THE SILICON ELECTROLYTE INTERFACE." <u>Journal of Physics-Condensed Matter</u> **5**: A133-A134.

Merlos, A., M. Acero, et al. (1993). "TMAH/IPA ANISOTROPIC ETCHING CHARACTERISTICS." <u>Sensors and Actuators a-Physical</u> **37-8**: 737-743.

Moore, G. E. (1965). "Cramming more components onto integrated circuits." <u>Electronics</u> **38**(8).

Outemzabet, R., N. Gabouze, et al. (2005). "Random macropore formation in n-type silicon under front side illumination: correlation with anisotropic etching." <u>phys.stat.sol.</u> **(c) 2**(9): 3394-3398.

Peter, L. M., D. J. Riley, et al. (1995). "IN-SITU MONITORING OF INTERNAL SURFACE-AREA DURING THE GROWTH OF POROUS SILICON." <u>Applied Physics Letters</u> **66**(18): 2355-2357.

Pierret, R. F. (1996). <u>Semiconductor Device Fundamentals</u>, Addison-Wesley.

Raz, O., Z. Shmueli, et al. (2010). "Porous Silicon Formation in Fluorohydrogenate Ionic Liquids." <u>Journal of the Electrochemical Society</u> **157**(3): H281-H286.

Rodin, A. M., J. Callaghan, et al. (2008). <u>High Throughput Low CoO Industrial Laser Drilling Tool</u>. 4th International Conference and Exhibition on Device Packaging, Arizona, USA.

Saadaoui, M., W. Wien, et al. (2008). <u>New Front To Back-side 3D Interconnects Based High Aspect Ratio Through Silicon Vias</u>. Electronics Packaging Technology Conference, 2008. EPTC 2008. 10th.

Sammak, A., S. Azimi, et al. (2007). "Deep vertical etching of silicon wafers using a hydrogenation-assisted reactive ion etching." <u>Journal of Microelectromechanical Systems</u> **16**(4): 912-918.

Sammak, A., S. Azimi, et al. (2007). <u>Silicon nanowire fabrication using novel hydrogenation-assisted deep reactive ion etching</u>. Semiconductor Device Research Symposium, 2007 International.

Sato, N. (1998). <u>Electrochemistry at metal and semiconductor electrodes</u>, Elsevier Science.

Savir, E., A. Many, et al. (1995). "Space-charge layers and surface states at the silicon/electrolyte interface." <u>Surface Review and Letters</u> **2**(6): 765-772.

Sekiguchi, M., H. Numata, et al. (2006). Novel low cost integration of through chip interconnection and application to CMOS image sensor. Electronic Components and Technology Conference, 2006. Proceedings. 56th.

SEMATECH. "http://www.sematech.org/research/3D/index.htm."

Tao, Y. and M. Esashi (2005). "Macroporous silicon-based deep anisotropic etching." Journal of Micromechanics and Microengineering **15**(4): 764-770.

VirginiaSemiconductor.

W., L. H., P. G. J., et al. (1995). "High aspect raio submicron pillars fabricated by photoassisted electrochemical etching and oxidation." Applied Physics Letters **67**(13): 3.

Wehrspohn, R. B., S. L. Schweizer, et al. (2007). "Linear and non-linear optical experiments based on macroporous silicon photonic crystals." Physica Status Solidi a-Applications and Materials Science **204**(11): 3708-3726.

Więckowski, A. (1999). Interfacial Electrochemistry: Theory, Experiment and Applications, Marcel Dekker Inc.

Woodruff, J. H., J. B. Ratchford, et al. (2007). "Vertically oriented germanium nanowires grown from gold colloids on silicon substrates and subsequent gold removal." Nano Letters **7**(6): 1637-1642.

Wu, B. Q., A. Kumar, et al. (2010). "High aspect ratio silicon etch: A review." Journal of Applied Physics **108**(5).

Zhang, X. G. (1991). "MECHANISM OF PORE FORMATION ON N-TYPE SILICON." Journal of the Electrochemical Society **138**(12): 3750-3756.

Zhang, X. G. (2004). "Morphology and Formation Mechanisms of Porous Silicon." Journal of the Electrochemical Society **151**(1): C69-C80.

Zhao, Z., J. Guo, et al. (2010). "Photoelectrochemical etching of uniform macropore array on full 5-inch silicon wafers." Journal of Semiconductors **31**(7).

APPENDIX. APPROVED PERMISSIONS FOR REUSE OF PUBLISHED MATERIALS

Dear Sir/Madam

I am a graduate student from Louisiana State University. I would like to request for the copyright for a figure to be used in my thesis.

Journal - J. Micromech. Microeng. **15** (2005) 764–770

Title - Macroporous silicon-based deep anisotropic etching

Author - Tao Y, Esashi M

Figure - Figure 1. Macropore formation using (1 0 0) n-type silicon anodization with backside illumination in an HF-based electrolyte

Thanking you.

Sincerely,

Purnima Narayanan

MS ChE

Louisiana State University.

PERMISSION TO REPRODUCE AS REQUESTED IS GIVEN PROVIDED THAT:

(a) the consent of the author(s) is obtained
(b) the source of the material including author, title of article, title of journal, volume number, issue number (if relevant), page range (or first page if this is the only information available), date and publisher is acknowledged.
(c) for material being published electronically, a link back to the original article should be provided (via DOI).

IOP Publishing Ltd
Dirac House
Temple Back
BRISTOL   11/4/2011
BS1 6BE   Date   Rights & Permissions

Dear Sir/Madam,

I am a graduate student from Louisiana State University. I would like to request for the copyright for a figure to be used in my thesis.

Journal - J. Micromech. Microeng. **15** (2005) 764–770

Title - Macroporous silicon-based deep anisotropic etching

Author - Tao Y, Esashi M

Figure - Figure 4. Overetching at the edge of macropore arrays
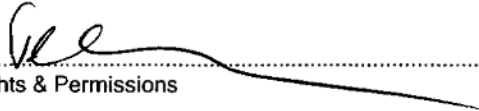
Thanking you.

Sincerely,

Purnima Narayanan

MS ChE

Louisiana State University.

PERMISSION TO REPRODUCE AS REQUESTED IS GIVEN PROVIDED THAT:

(a) the consent of the author(s) is obtained
(b) the source of the material including author, title of article, title of journal, volume number, issue number (if relevant), page range (or first page if this is the only information available), date and publisher is acknowledged.
(c) for material being published electronically, a link back to the original article should be provided (via DOI).

IOP Publishing Ltd
Dirac House
Temple Back
BRISTOL   11/4/2011
BS1 6BE   Date   Rights & Permissions

I am a graduate student from Louisiana State University. I would like to request for the copyright for a figure from the following journal to be used in my thesis.

Journal - J. Micromech. Microeng. 19 (2009) 095009 (11pp)

Title - Formation of deep periodic trenches in photo-electrochemical etching of n-type silicon

Author - E V Astrova and G V Fedulova

Figure - **Figure 10.** SEM of (a) pores in silicon walls for a sample etched at a high current density: cross-section of structure 14NSa7

Thanking you in anticipation.

Sincerely,

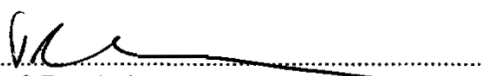Purnima Narayanan.

MS ChE

Louisiana State University.
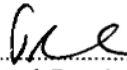
Ph: 225-223-3363

PERMISSION TO REPRODUCE AS REQUESTED IS GIVEN PROVIDED THAT:

(a) the consent of the author(s) is obtained
(b) the source of the material including author, title of article, title of journal, volume number, issue number (if relevant), page range (or first page if this is the only information available), date and publisher is acknowledged.
(c) for material being published electronically, a link back to the original article should be provided (via DOI).

IOP Publishing Ltd
Dirac House
Temple Back
BRISTOL   7/4/2011
BS1 6BE   Date   Rights & Permissions

Dear Customer,

Thank you for your email.

We hereby grant permission for the requested use expected that due credit is given to the original source.

If material appears within our work with credit to another source, authorisation from that source must be obtained.

Credit must include the following components:

- Books: Author(s)/ Editor(s) Name(s): Title of the Book. Page(s). Publication year. Copyright Wiley-VCH Verlag GmbH & Co. KGaA. Reproduced with permission.

- Journals: Author(s) Name(s): Title of the Article. Name of the Journal. Publication year. Volume. Page(s). Copyright Wiley-VCH Verlag GmbH & Co. KGaA. Reproduced with permission.

 With kind regards

Bettina Loycke

****

Bettina Loycke

Senior Rights Manager

Wiley-VCH Verlag GmbH & Co. KGaA

Boschstr. 12

69469 Weinheim

Germany

Phone: +49 (0) 62 01- 606 - 280

Fax: +49 (0) 62 01 - 606 - 332

Email: rights@wiley-vch.de

_____

Wiley-VCH Verlag GmbH & Co. KGaA

Location of the Company: Weinheim

Chairman of the Supervisory Board: Stephen Michael Smith

Trade Register: Mannheim, HRB 432833

General Partner: John Wiley & Sons GmbH, Location: Weinheim

Trade Register Mannheim, HRB 432296

Managing Directors : Christopher J. Dicks, Bijan Ghawami, William Pesce

From: Purnima Narayanan [mailto:p1@tigers.lsu.edu]

Sent: Thursday, April 07, 2011 4:03 PM

To:Permissions - US

Subject: Request for copyright permission

Dear Sir/Madam

I am a graduate student from Louisiana State University. I would like to request for the copyright for a figure to be used in my thesis.

Journal - phys. stat. sol. (c) 2, No. 9, 3394–3398 (2005) / DOI 10.1002/pssc.200461185

Title - Random macropore formation in n-type silicon under front side illumination: correlation with anisotropic etching

Author - R. Outemzabet, N. Gabouze, N. Kesri, and H. Cheraga

Figure - Fig. 5 Integrated infrared absorbance as a function of applied potential for p-Si: a) vOH region, vSiH and vSi-O vibrations of Si (100) oriented

Thanking you.

Sincerely,

Purnima Narayanan

MS ChE

Louisiana State University.

Comments/Response to Case ID:

ReplyTo:

From: Jacqueline Hansson   Date: 05/02/2011

Subject: Re: Request for   Send To: Purnima Narayanan

copyright permission   <p1@tigers.lsu.edu>

cc:

Dear Purnima Narayanan :

We are happy to grant you permission to reuse the IEEE copyrighted figure

requested in all electronic and printed formats.

Since the figures are for use in your thesis, our only requirements are

that you credit the original source (author, paper, and publication), and

that the IEEE copyright line (© 2010 IEEE) appears prominently with the

reprinted figure.

Sincerely,

Jacqueline Hansson, Coordinator

© © © © © © © © © © © © © © © © © © ©

 IEEE Intellectual Property Rights Office

445 Hoes Lane

Piscataway, NJ 08855-1331 USA

+1 732 562 3966 (phone)

+1 732 562 1746 (fax)

IEEE-- Fostering technological innovation

and excellence for the benefit of humanity.

© © © © © © © © © © © © © © © © © © ©

Dear Sir/Madam,

I am a graduate student from Louisiana State University. I would like to request permission for using a figure from the following publication in my thesis:

* Fig. 3 *(a) FIB pictures of DRIE Si via etching;

Title: Design, fabrication and electrical characterization of TSV

Publication: IEEE Conference Proceedings

Publisher: IEEE

Date: an 1, 2010

Thanking You.

Sincerely,

Purnima Narayanan.

MS ChE

Louisiana State University.

This is a License Agreement between Purnima Narayanan ("You") and Elsevier ("Elsevier") provided by Copyright Clearance Center ("CCC"). The license consists of your order details, the terms and conditions provided by Elsevier, and the payment terms and conditions.

All payments must be made in full to CCC. For payment instructions, please see information listed at the bottom of this form.

Supplier	Elsevier Limited The Boulevard,Langford Lane Kidlington,Oxford,OX5 1GB,UK
Registered Company Number	1982084
Customer name	Purnima Narayanan
Customer address	3650 Nicholson Dr.
	baton Rouge, LA 70802
License number	2665150368039
License date	May 10, 2011
Licensed content publisher	Elsevier
Licensed content publication	Surface Science
Licensed content title	Etching of silicon in fluoride solutions
Licensed content author	Kurt W. Kolasinski
Licensed content date	1 June 2009
Licensed content volume number	603
Licensed content issue number	10-12
Number of pages	8
Start Page	1904
End Page	1911
Type of Use	reuse in a thesis/dissertation
Portion	figures/tables/illustrations
Number of figures/tables/illustrations	3
Format	both print and electronic
Are you the author of this Elsevier article?	No

Will you be translating?	No
Order reference number	
Title of your thesis/dissertation	PHOTOELECTROCHEMICAL ETCHING OF ISOLATED, HIGH ASPECT RATIO MICROSTRUCTURES IN n-TYPE SILICON (100)
Expected completion date	Aug 2011
Estimated size (number of pages)	80
Elsevier VAT number	GB 494 6272 12
Permissions price	0.00 USD
VAT/Local Sales Tax	0.0 USD / 0.0 GBP
Total	0.00 USD
Terms and Conditions	

altered/adapted minimally to serve your work. Any other abbreviations, additions, deletions and/or any other alterations shall be made only with prior written authorization of Elsevier Ltd. (Please contact Elsevier at permissions@elsevier.com)

6. If the permission fee for the requested use of our material is waived in this instance, please be advised that your future requests for Elsevier materials may attract a fee.

7. Reservation of Rights: Publisher reserves all rights not specifically granted in the combination of (i) the license details provided by you and accepted in the course of this licensing transaction, (ii) these terms and conditions and (iii) CCC's Billing and Payment terms and conditions.

8. License Contingent Upon Payment: While you may exercise the rights licensed immediately upon issuance of the license at the end of the licensing process for the transaction, provided that you have disclosed complete and accurate details of your proposed use, no license is finally effective unless and until full payment is received from you (either by publisher or by CCC) as provided in CCC's Billing and Payment terms and conditions. If full payment is not received on a timely basis, then any license preliminarily granted shall be deemed automatically revoked and shall be void as if never granted. Further, in the event that you breach any of these terms and conditions or any of CCC's Billing and Payment terms and conditions, the license is automatically revoked and shall be void as if never granted. Use of materials as described in a revoked license, as well as any use of the materials beyond the scope of an unrevoked license, may constitute copyright infringement and publisher reserves the right to take any and all action to protect its copyright in the materials.

9. Warranties: Publisher makes no representations or warranties with respect to the licensed material.

10. Indemnity: You hereby indemnify and agree to hold harmless publisher and CCC, and their respective officers, directors, employees and agents, from and against any and all claims arising out of your use of the licensed material other than as specifically authorized pursuant to this license.

11. No Transfer of License: This license is personal to you and may not be sublicensed, assigned, or transferred by you to any other person without publisher's written permission.

12. No Amendment Except in Writing: This license may not be amended except in a writing signed by both parties (or, in the case of publisher, by CCC on publisher's behalf).

13. Objection to Contrary Terms: Publisher hereby objects to any terms contained in any purchase order, acknowledgment, check endorsement or other writing prepared by you, which terms are inconsistent with these terms and conditions or CCC's Billing and Payment terms and conditions. These terms and conditions, together with CCC's Billing and Payment terms and conditions (which are incorporated herein), comprise the entire agreement between you and publisher (and CCC) concerning this licensing transaction. In the event of

any conflict between your obligations established by these terms and conditions and those established by CCC's Billing and Payment terms and conditions, these terms and conditions shall control.

14. Revocation: Elsevier or Copyright Clearance Center may deny the permissions described in this License at their sole discretion, for any reason or no reason, with a full refund payable to you. Notice of such denial will be made using the contact information provided by you. Failure to receive such notice will not alter or invalidate the denial. In no event will Elsevier or Copyright Clearance Center be responsible or liable for any costs, expenses or damage incurred by you as a result of a denial of your permission request, other than a refund of the amount(s) paid by you to Elsevier and/or Copyright Clearance Center for denied permissions.

Dear Purnima Narayanan :

We are happy to grant you permission to reuse the IEEE copyrighted figures requested in all electronic and printed formats.

Since the figure is for use in your thesis, our only requirements are that you credit the original source (author, paper, and publication), and that the IEEE copyright line (© 2008 IEEE) appears prominently with each reprinted figure.

Sincerely,

Jacqueline Hansson, Coordinator

IEEE Intellectual Property Rights Office

445 Hoes Lane

Piscataway, NJ 08855-1331 USA

+1 732 562 3828 (phone)

+1 732 562 1746(fax)

e-mail: j.hansson@ieee.org

IEEE Fostering technological innovation

and excellence for the benefit of humanity.

©©©©©©©©©©©©©©©©©©©©©©©©©©©©©©©

From: Purnima Narayanan <p1@tigers.lsu.edu>

To: j.hansson@ieee.org, customercare@copyright.com

Date: 05/09/2011 11:41 PM

Subject: Request for copyright permission

Dear Sir/Madam,

I would like to get the copy right permission to use a figure from the following content in my Master's thesis.

But when I go through RightsLink; in the dropdown list for there is no option for " reuse in a thesis or dissertation" or "reuse in a manner not listed here" or "I don't see my intended use".

Could you please guide me to proceed to get the permission.

Title: 3D stacked IC demonstration using a through Silicon Via First approach

Publication: IEEE Conference Proceedings

Publisher: IEEE

Date: Jan 1, 2008

Fig 2&3: FIB through TSV in vicinity of device after etch, strip& clean (left), and after TSV CMP and sintering (right). (Pt on top for contrast)

Thanking You.

Sincerely,

Purnima Narayanan

MS ChE

Louisiana State University.

Request for Permission to Reproduce or Re-Publish ECS Material

Please fax this form to: The Electrochemical Society (ECS), Attn: Permissions Requests, 1.609.730.0629. You may also e-mail your request to: copyright@electrochem.org. Include all the information as required on this form. Please allow 3-7 days for your request to be processed.

I am preparing a (choose one): ☐ paper   ☐ chapter   ☐ book   ☑ thesis

entitled: FABRICATION OF THROUGH SILICON VIAS IN n-type Si(100)

to be published by: N/A

in an upcoming publication entitled: N/A.

I request permission to use the following material in the publication noted above, and request nonexclusive rights for all subsequent editions and in all foreign language translations for distribution throughout the world.

Description of material to be used—Indicate what material you wish to use (figures, tables, text, etc.) and give the full bibliographic reference for the source publication. You may attach a separate list, organized by ECS title.

JOURNAL OF THE ELECTROCHEMICAL SOCIETY, 147(2) 627-635 (2000)

AUTHORS: M. HEJJO AL RIFAI, M. CHRISTOPHERSEN, S. OTTOW, J. CARSTENSEN, H. FOLL

TITLE: DEPENDENCE OF MACROPORE FORMATION IN n-Si on POTENTIAL, TEMPERATURE AND DOPING ; FIGURE 14. REPLOTTING THE PORE DISTANCE VS ETCHING POTENTIAL.

Signature: Purnima.N   Date: 04/07/2011

Name: PURNIMA NARAYANAN

Address: 3650 NICHOLSON DR.

APT # 1147.

BATON ROUGE, LA - 70802

Telephone: 225-223-3363   Fax: —

E-mail: p1@tigers.lsu.edu

Permission is granted to reproduce the above-referenced material. Please acknowledge the author(s) and publication data of the original material, and include the words: "Reproduced by permission of The Electrochemical Society."

April 15, 2011
Date

Ann F. Goedkoop, Director of Publications

Purnima Narayanan

MS ChE

Louisiana State University.

Dear Purnima

Thank you for your request regarding image use in EuroAsia Magazine. I am more than happy to agree to the use of this image and am always happy to assist with continuing education. I have made a slight change to your copyright details and would request the following details be used.

Publisher: Angel Business Communications

Magazine   EuroAsia Semiconductor

Title: High Throughput Low CoO Industrial Laser Drilling Tool

Author: Alexey M.Rodin, Joseph Callaghan and Niall Brennan

XSil Ltd.

Year : July, 2008

Fig.2 SEM image: cross-sectioned line of 10μm diameter vias with ±0.8% depth variation

Good luck with your thesis. Would love to hear how it goes and even se a copy. Depending on the outcome for you I have ran précised versions of student thesis hwen appropriate.

Kindest regards

David

David Ridsdale

Editor in Chief

+44 (0)1923 690 200

Solar

http://www.solar-pv-management.com/

Compound Semiconductor

http://www.compoundsemiconductor.net

EuroAsia Semiconductor

http://www.euroasiasemiconductor.com

From: Purnima Narayanan [mailto:p1@tigers.lsu.edu]

Sent: 10 May 2011 05:11

To: Jackie Cannon

Subject: request for copyright permission

Dear Sir/Madam,

I would like to obtain the copy right permission to use a figure from the following content in my Master's thesis.

Publisher: EuroAsia Semiconductor

Title: High Throughput Low CoO Industrial Laser Drilling Tool

Author: Alexey M.Rodin, Joseph Callaghan and Niall Brennan

XSil Ltd.

Year : July, 2008

Fig.2 SEM image: cross-sectioned line of 10μm diameter vias with ±0.8% depth variation

Thanking You.

Sincerely,

Purnima Narayanan

MS ChE

Louisiana State University

VITA

Purnima Narayanan was born in the city of Mumbai, India, in 1985. She obtained her Bachelor of Engineering in Chemical Engineering degree from University of Mumbai in July 2007. In August 2008, she came to Louisiana State University to pursue a Master of Science in Chemical Engineering degree.